Research progress on geosynchronous synthetic aperture radar

Hu, Cheng; Chen, Zhiyang; Li, Yuanhao; Dong, Xichao; Hobbs, Stephen

DOI
10.1016/j.fmre.2021.04.008

Publication date
2021

Document Version
Final published version

Published in
Fundamental Research

Fundamental Research 1 (2021) 346–363

Contents lists available at ScienceDirect

Fundamental Research

journal homepage: http://www.keaipublishing.com/en/journals/fundamental-research/

Review

Research progress on geosynchronous synthetic aperture radar

Cheng Hu[a,b,1,*], Zhiyang Chen[a,c,1], Yuanhao Li[d], Xichao Dong[a,e], Stephen Hobbs[f]

[a] The School of Information and Electronics, Beijing Institute of Technology, Beijing 100081, China
[b] Advanced Technology Research Institute, Beijing Institute of Technology, Jinan 250300, China
[c] The Key Laboratory of Electronic and Information Technology in Satellite Navigation (Beijing Institute of Technology), Ministry of Education, Beijing 100081, China
[d] Department of Geoscience and Remote Sensing, Delft University of Technology, 2628 Delft, the Netherlands
[e] Beijing Institute of Technology Chongqing Innovation Center, Chongqing 401120, China
[f] The School of Aerospace Transport & Manufacturing, Cranfield University, UK

ARTICLE INFO

Keywords:
Geosynchronous synthetic aperture radar (GEO SAR)
Orbit scheme
Disturbance factors
Echo focusing
Formation flying

ABSTRACT

Based on its ability to obtain two-dimensional (2D) high-resolution images in all-time and all-weather conditions, spaceborne synthetic aperture radar (SAR) has become an important remote sensing technique and the study of such systems has entered a period of vigorous development. Advanced imaging modes such as radar interferometry, tomography, and multi-static imaging, have been demonstrated. However, current in-orbit spaceborne SARs, which all operate in low Earth orbits, have relatively long revisit times ranging from several days to dozens of days, restricting their temporal sampling rate. Geosynchronous SAR (GEO SAR) is an active research area because it provides significant new capability, especially its much-improved temporal sampling. This paper reviews the research progress of GEO SAR technologies in detail. Two typical orbit schemes are presented, followed by the corresponding key issues, including system design, echo focusing, main disturbance factors, repeat-track interferometry, etc, inherent to these schemes. Both analysis and solution research of the above key issues are described. GEO SAR concepts involving multiple platforms are described, including the GEO SAR constellation, GEO-LEO/airborne/unmanned aerial vehicle bistatic SAR, and formation flying GEO SAR (FF-GEO SAR). Due to the high potential of FF-GEO SAR for three-dimensional (3D) deformation retrieval and coherence-based SAR tomography (TomoSAR), we have recently carried out some research related to FF-GEO SAR. This research, which is also discussed in this paper, includes developing a formation design method and an improved TomoSAR processing algorithm. It is found that GEO SAR will continue to be an active topic in the aspect of data processing and multi-platform concept in the near future.

1. Introduction

Synthetic aperture radar (SAR) is an active microwave imaging sensor mounted on a moving platform that can be used to obtain high-resolution images day and night and in all-weather conditions [1]. Spaceborne SAR plays irreplaceable roles in the fields of military reconnaissance [2], environment remote sensing [3], disaster monitoring [4], etc. Since SEASAT, the first spaceborne SAR, was launched by the U.S.A. in 1978 [5], spaceborne SAR has become a leading research area in the field of Earth observation. In the 21st century, many countries and organizations have deployed their own spaceborne SAR systems and even implemented upgrades to such systems. For example, the European Space Agency (ESA) has launched Sentinel-1 to succeed ENVISAT [6]. Based on the successful implementation and outstanding application performance of TanDEM-X, the German Aerospace Center (DLR) is expected to launch TanDEM-L [7] in approximately 2022 to monitor the dynamic changes in the Earth system based on the high penetration of the L-band signal.

At present, in-orbit spaceborne SARs all operate in low Earth orbits (LEO, with altitudes that are typically lower than 1000 km); these SARs have global coverage capabilities, but their performance for revisiting a given region is not good enough for some users. The revisit period of LEO SAR is typically slightly more than ten days, and sometimes even up to dozens of days, causing severe temporal decorrelation. Geosynchronous SAR (GEO SAR) operates in an orbit with an altitude of approximately 36000 km, which has a revisit period of one (sidereal) day, much shorter than that of LEO SAR. In addition, GEO SAR enables beam coverage of up to thousands of kilometers; therefore, it can be used to effectively realize large-scale and near-continuous observations, which is a capability that is urgently needed for military and disaster monitoring [8]. In

* Corresponding author.
E-mail address: cchchb@bit.edu.cn (C. Hu).
[1] These authors contributed equally to this work.

https://doi.org/10.1016/j.fmre.2021.04.008

Available online 4 May 2021

this paper, progresses in researching GEO SAR techniques are reviewed. First, two typical GEO SAR orbit schemes are presented, including the inclined orbit and the near-zero inclination orbit. Second, the key issues that have attracted much attention in recent years, such as system design, echo focusing, main disturbance factors, and repeat-track interferometry, are described. Third, GEO SAR concepts involving multiple platforms, including constellation, GEO-LEO/airborne/unmanned aerial vehicle bistatic SAR, and GEO SAR exploiting formation flying (FF-GEO SAR), are reviewed. We also discuss research we have conducted recently regarding FF-GEO SAR, namely, the formation design method, performance analysis and an improved coherence-based SAR tomography (TomoSAR) processing algorithm. Finally, the paper is concluded, and visions for future GEO SAR research are discussed.

2. GEO SAR orbit schemes

At present, the mainstream GEO SAR concepts mainly include near-zero inclination GEO SARs and inclined GEO SARs [9], as shown in Fig. 1 (a). Among the latter schemes, high- and medium-inclination schemes are popular research topics, in which the shapes of the nadir-point trajectories are large and small "figure 8" shapes, respectively. The inclined schemes have mainly been studied by scholars from the U.S.A. and China, while most work on near-zero inclination schemes has been carried out by European scholars.

2.1. Near-zero inclination (NZI) GEO SAR

The NZI GEO SAR scheme was first proposed by Tomiyasu from the National Aeronautics and Space Administration (NASA) of the U.S.A. in 1978 [10], and this proposal was also the first public report on the GEO SAR concept. He proposed that with the key orbital elements of 1° inclination, 90° argument of perigee (AoP) and 0.009 eccentricity, GEO SAR has a nearly circular nadir-point trajectory. GEO SAR has an effective velocity (the platform's velocity relative to the target) of 48 m/s, which can enable a 100 m resolution SAR image to be obtained in an integration time of 700 s. With an L-band radar, the whole North America continent can be imaged in 4 hours by switching footprints at a resolution of 100 m.

Since 1998, European scholars, represented by scientists in Italy, the U.K. and Spain, have begun to study NZI GEO SAR [11–15]; at first, they mainly considered passive systems. Scholars from Politecnico di Milano (POLIMI) in Italy, namely C. Prati and F. Rocca, conceived the idea to place a receiver with a small eccentricity in geosynchronous orbit to receive backscattered audio broadcast signals. The receiver's effective velocity was approximately only 2 m/s. Using a 4.8 m antenna, images with a resolution of 120 m could be obtained for a 1500 km scene [11], but the integration time was up to 8 hours. Later, European scholars switched over to studying active GEO SARs. In 2013, J. R. Rodon et al. from Universitat Politècnica de Catalunya (UPC) proposed that NZI GEO SAR could be used to retrieve atmospheric phase screens (APSs) [16]. A. V. Monti-Guarnieri from POLIMI and S. Hobbs from Cranfield University (CU) proposed an NZI GEO SAR scheme and submitted it to the Earth Explorer (EE) program of ESA, including EE-9 and EE-10 [17,18], which were intended for topographic/atmospheric observation and hydrosphere observation, respectively. Among them, the scheme in EE-10 (G-CLASS, now renamed Hydroterra) became one of the three candidate projects [19]. It is proposed to place a GEO SAR over the African continent using a C-band antenna with a diameter of about 7 m. Hydroterra is intended for hourly to daily observation of water cycle processes over Europe and Africa, especially the periphery of the Mediterranean Sea,

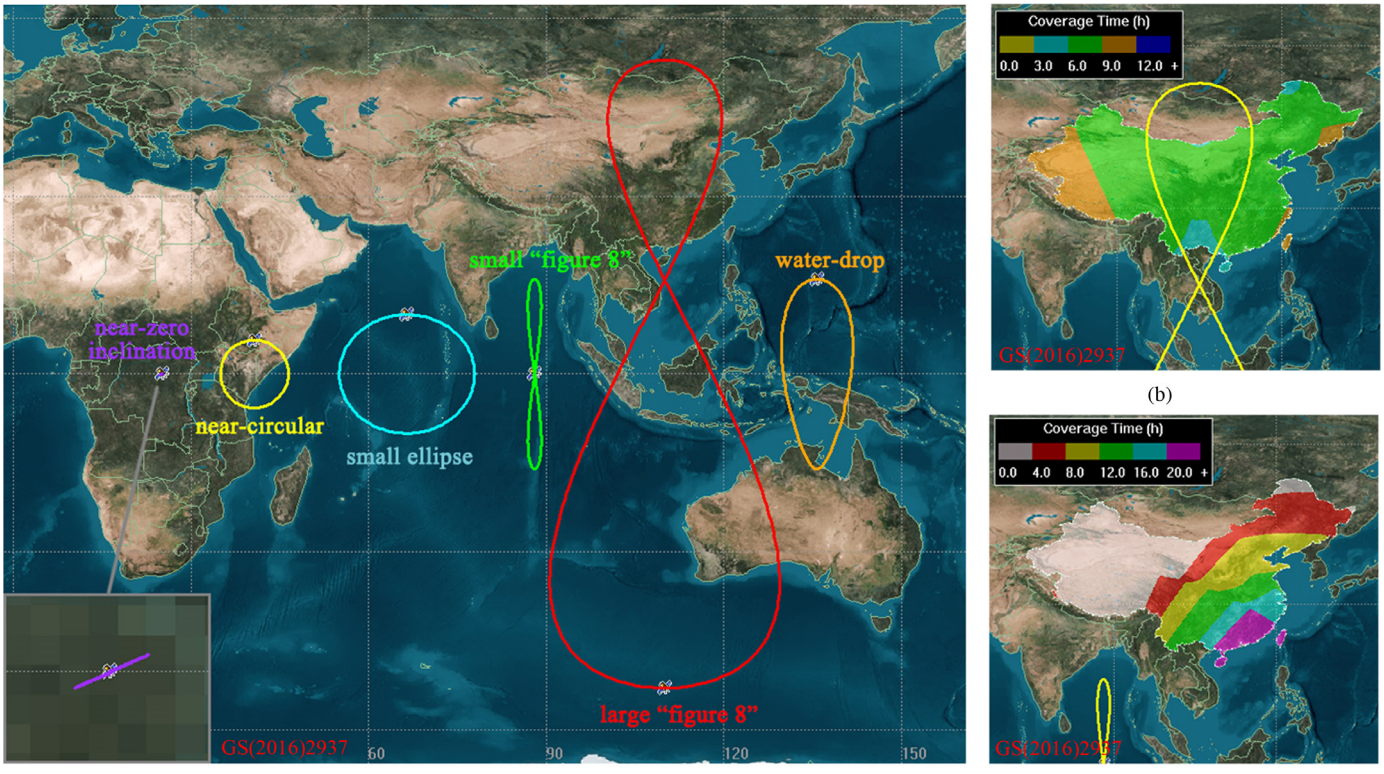

Fig. 1. GEO SAR orbit schemes and coverage performances of some of these schemes. (a) Nadir-point trajectories of GEO SAR orbit schemes. (b) 53° and (c) 16° inclination GEO SAR's coverage performances in China.

so as to explore hydrological phenomena including intense rainfall and the surface water budget [20].

2.2. Inclined GEO SAR

Realizing that the effective velocity of the GEO SAR scheme previously proposed in 1978 implied restricted geographical coverage, Tomiyasu proposed a new GEO SAR scheme with 50° inclination to image the entire U.S. region in 1983 [21]. Compared with the original scheme, this scheme had a nadir-point trajectory in a large "figure 8" shape, and thus, it had a shorter integration time and a larger coverage. However, due to the large required antenna (15 m or 30 m) and high average transmission power (more than 1 kW RF), it could not be realized through engineering capabilities at that time. This limitation directly led to slow research progress in the system design and key technology of inclined GEO SARs for the next 20 years.

Since 2000, with the rapid development of electronic technology, research on large antennas and high-power transmit/receive (T/R) module technology has made rapid progress, and thus, many studies of inclined GEO SAR have gained momentum again. In 2001, researchers at the Jet Propulsion Laboratory (JPL) in the U.S.A. pointed out that a GEO SAR with a large inclination (50°-65°) had great application prospects in disaster management, tectonic mapping and modeling. [22]. These scientists initially demonstrated the system requirements, including the power and antenna size requirements, and believed that the main technical difficulties that limited the realization of the scheme included the average transmission power of 15 kW and the 30 m aperture antenna. On the basis of this work, JPL proposed the Global Earthquake Satellite System (GESS, see the GEO SAR Constellation section below) in 2003 [23]. Ten inclined GEO SAR satellites were divided into five groups to achieve global coverage. Since then, American scholars have seldom published research on GEO SAR.

Another team actively conducting research on GEO SAR comes from China. Since 2007, scholars from the China Academy of Space Technology (CAST) and Beijing Institute of Technology (BIT) have jointly studied inclined GEO SARs [13]. Taking into account China's large latitude and longitude ranges, they first adopted a GEO SAR with a high inclination of more than 50°, which had a large "figure 8" shape of nadir-point trajectory, to cover major areas of China. They set the apogee of the orbit to be at the North Pole (i.e., the position at which the argument of latitude (AoL) is 90°) to obtain a longer observation time for the Northern Hemisphere [24]. Furthermore, the BIT team found that such a high-inclination GEO SAR scheme could provide multiple observation angles for many areas. Therefore, one potential application of highly inclined GEO SAR is three-dimensional (3D) deformation retrieval based on multiangle observations. By selecting the optimal combination of observation angles, a theoretical 3D deformation retrieval accuracy better than 2 cm was achieved for western China [24]. Recently, medium-inclination (16°) GEO SAR, whose nadir-point trajectory is a small "figure 8" shape, has become a popular topic of research due to a longer coverage time for China [24,25] (see Fig. 1 (b) and (c)); medium-inclination GEO SAR is currently also the main configuration adopted for theoretical research.

2.3. Other schemes

In addition to the abovementioned mainstream orbit schemes, Chinese scholars have also proposed a variety of configurations to enable special applications or specific observation performances, such as GEO circular SAR, which can realize 3D imaging [26], and GEO SAR with a small ellipse nadir-point track, which has good coverage performance for China via a left-looking mode [27] and a "water-drop" nadir-point track [28]. In some scholars' research on focusing algorithms or system analyses, one or more of these configurations have been selected to verify the proposed methods.

3. Key Issues in GEO SAR

Both the advantages and challenges of GEO SAR come from its much higher orbit than LEO SAR. Compared to LEO SAR, the orbit height of GEO SAR is two orders of magnitude larger. Accordingly, the Earth rotation effect [29], signal propagation distance [29], synthetic aperture time and imaging swath [30] are enhanced or enlarged to the same degree, the influence of which will be briefly stated herein. Due to this much more severe Earth rotation effect, the resolution analysis method [29], beam/attitude control method [29] and sensitivity analysis method [27] of traditional LEO SAR fail in GEO SAR. The long-range results in a round-trip time for the signal of 0.25 s, and hundreds of seconds results in a significantly non-linear trajectory. In terms of range history modeling, these two factors invalidate the "stop-go" assumption and straight-trajectory-based range model widely adopted in LEO SAR. Furthermore, the GEO SAR signal is affected by a temporally and spatially variant atmosphere because of the long integration time and extent of beam coverage. In addition, the curve trajectory also leads to nonparallel repeat tracks, which results in the failure of the traditional height-retrieval elevation model and causes rotation-induced decorrelation for a GEO SAR interferometry (InSAR) pair. This decorrelation, in turn, deteriorates the performances of InSARs and differential InSARs (D-InSARs). The abovementioned main issues in GEO SAR are shown in Fig. 2.

3.1. System design

A GEO SAR (especially the NZI) has a practically permanent view of the Earth disk. This means that a given area can be imaged at almost any time during the day. In general, the radar will not image in the usual LEO "zero Doppler" configuration, and so lines of constant range and constant Doppler are not always orthogonal. The viewing geometry also affects polarimetry. The "natural" linear polarization directions for the satellite are North and East. The conversion of these into local vertical and horizontal polarization directions requires a coordinate rotation which depends on the target location. For interferometry, the orbit track should repeat within tight limits for coherent imaging, and therefore the standard temporal baseline is integer multiples of one sidereal day. Since sidereal and solar days differ by about 4 minutes, the solar time of coherent images shifts by about 2 hours per month and this shift has to be accounted for in operations planning. Orbit maintenance needs care-

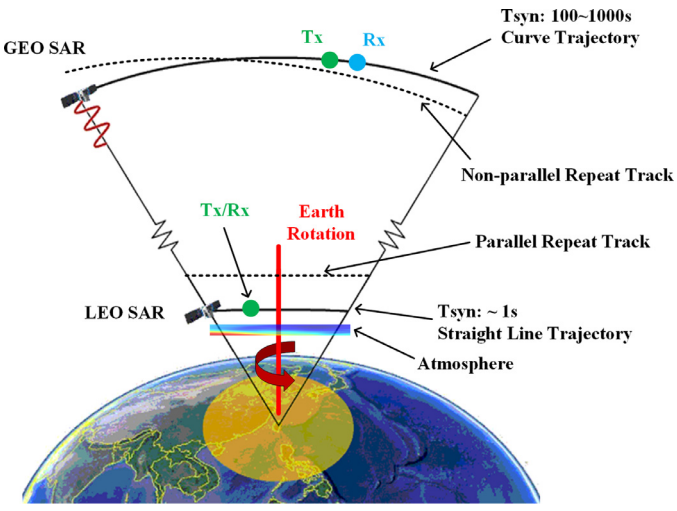

Fig. 2. Illustration of main challenges in GEO SAR, as presented by a comparison to LEO SAR, where Tsyn represents synthetic aperture time. The "stop-go" assumption in LEO SAR means the platform is considered stationary during a signal pulse's propagation.

ful planning to minimize fuel consumption while achieving good orbit repeat geometry for interferometry.

In terms of GEO SAR system parameter analysis and design, European scholars have mainly focused on the comprehensive consideration of both performance requirements and engineering implementation techniques. In 2006, S. Hobbs briefly presented the main factors of GEO SAR engineering design in the form of a group design project, covering all the major aspects of spaceborne SAR engineering implementation, including considerations for the budget, antenna, power, communication, launch, etc. [12]. In 2014, S. Hobbs proposed a GEO SAR system parameter design process consisting of two main steps [9], in which the first step involved the determination of the wavelength, integration time and resolution, and the second step involved calculations for the required antenna size and power to ensure the signal-to-noise ratio (SNR) constraint were met. J. Ruiz-Rodon et al. further discussed the system design of NZI GEO SAR. Starting from a consideration of the eccentricity impacts on the resolution, they presented a design method for power and pulse-repetition frequency (PRF) and discussed the orbit station-keeping requirements for D-InSAR [31].

Since Chinese scholars' research on GEO SAR has focused on the inclined scheme, which is limited by Earth rotation more than NZI rotation, they have given more consideration to the impacts of the Earth's rotation on the GEO SAR system design. In 2011, C. Hu et al. from BIT described the Earth rotation effect on GEO SAR resolution. By deriving the generalized ambiguity function (GAF) of GEO SAR, they concluded that the Doppler gradient in the GAF was significantly affected by the Earth's rotation, which led to the apparent nonorthogonality of the GAF sidelobes on the ground; thus, the iso-range and iso-Doppler resolution directions on the ground were nonorthogonal [29]. Furthermore, analytical expressions for the iso-range and iso-Doppler resolutions were provided, while for an arbitrary direction, one can evaluate the resolution by solving the GAF equation numerically [29].

In addition, the Earth's rotation yields a nonzero-Doppler centroid for GEO SAR that cannot be eliminated in nonzero eccentricity GEO SAR by the conventional one-dimensional (1D) attitude control method [32]. Subsequently, a variety of attitude control and beam scan methods were proposed for performance optimization, including a two-dimensional (2D) phase scan method that was used to achieve a zero-Doppler centroid [32], an attitude steering method that enabled optimal ground resolution [33], and a joint attitude control and beam scan method that was used to realize the staring mode [34]. The Earth's rotation also affects the GEO SAR SNR in that it induces nonorthogonality in the 2D resolution directions, increasing the resolution cell area; thus, a larger transmission power is needed to satisfy the same resolution requirements [27].

3.2. Echo focusing

The trajectory characteristics of GEO SAR induce three main problems regarding echo focusing: the "stop-go" assumption error, curve trajectory, and large equivalent squint angle. In particular, the inclined GEO SAR studied by Chinese scholars has a more complex trajectory, and thus echo focusing is more challenging. Therefore, the research on the GEO SAR echo focusing algorithm mainly comes from China.

3.2.1. Accurate signal modeling

The "stop-go" assumption error originates from the satellite motion during the round-trip signal propagation, a phenomenon which cannot be ignored for the very long-range case (e.g., GEO SAR) or the very high-angular-velocity platform case (e.g., missile-borne SAR [35]). In 2011, the BIT team modeled the GEO SAR "stop-go" assumption error for the first time [29]. Assuming that the movements of the platform and the target are uniform linear motions during the round trip of a signal pulse (where the target motion is caused by the Earth's rotation), the error can be analytically expressed based on the platform's effective velocity and the range vector. Since both variables vary with slow time, the "stop-go" assumption error can be modeled by a high-order Taylor expansion of slow time.

To achieve a close or even better resolution performance as compared to LEO SAR, the synthetic aperture time of GEO SAR reaches hundreds of seconds. For a medium-inclination GEO SAR scheme with a small "figure 8" shape in the nadir-point trajectory, 1000 s of integration time is needed to obtain an azimuth-imaging resolution of 5 m at the orbit position above the equator. Long integration time yields the curve trajectory, resulting in a severe 2D spatial variation in the focusing parameters and range cell migration (RCM). There are two methods that can be used to solve this problem. One such method involves correcting the curve trajectory into a straight track during the imaging process [36]. However, only a very narrow swath can be accurately focused with this method, so the whole scene needs to be divided into very small segments that are each focused separately, significantly increasing the computational burden.

At present, the other method, that is, using high-order Taylor expansion to model the range history, has been widely adopted. For GEO SAR with an integration time less than 1000 s, combining the "stop-go" assumption error, a fourth-order curve trajectory model and a third-order "stop-go" error model are usually used to accurately model the range history [30], and the range can be expressed as

$$r(t_n) \approx (r_0 + \Delta r_0) + (k_1 + \Delta k_1)t_n + (k_2 + \Delta k_2)t_n^2 + (k_3 + \Delta k_3)t_n^3 + k_4 t_n^4, \tag{1}$$

where $t_n \in [-T_s/2, T_s/2]$, T_s is the integration time, k_i and Δk_i are the coefficients for fitting the curve trajectory and the "stop-go" error, respectively. r_0 is the range at $t_n = 0$ under "stop-go" assumption, Δr_0 is the "stop-go" error at $t_n = 0$. When the integration time is further increased at some orbit positions, it is necessary to use a fifth-order Taylor expansion to model the range history [37]. Nevertheless, generally speaking, the range model of the fourth-order Taylor expansion is sufficiently accurate in most cases. The high-order coefficient of the range history makes the derivation of the corresponding analytical 2D spectrum very difficult. To solve this problem, a method based on series inversion and the principle of stationary phase is generally adopted [38,39]. If we combine coefficients of the same order in (1), i.e., denoting $R_0 = r_0 + \Delta r$, $K_i = k_i + \Delta k_i, i = 1, 2, 3$, and $K_4 = k_4$, then the 2D spectrum can be expressed as

$$\begin{aligned} s(f_r, f_a) = {} & \sigma A_r(f_r) A_a(f_a) \exp\left(-j\pi \frac{f_r^2}{\beta}\right) \times \exp\left(-j2\pi \frac{2(f_r + f_c)}{c} R_0\right) \\ & \times \exp\left(j2\pi \frac{1}{4K_2} \frac{c}{2(f_r + f_c)} \left[f_a + \frac{2K_1 \cdot (f_r + f_c)}{c}\right]^2\right) \\ & \times \exp\left(j2\pi \frac{K_3}{8K_2^3} \left[\frac{c}{2(f_r + f_c)}\right]^2 \cdot \left[f_a + \frac{2K_1 \cdot (f_r + f_c)}{c}\right]^3\right) \\ & \times \exp\left(j2\pi \frac{9K_3^2 - 4K_2K_4}{64K_2^5} \cdot \left[\frac{c}{2(f_r + f_c)}\right]^3 \right. \\ & \left. \times \left[f_a + \frac{2K_1 \cdot (f_r + f_c)}{c}\right]^4\right), \end{aligned} \tag{2}$$

where c is the speed of light and σ is the amplitude. $A_r(f_r)$ and $A_r(f_a)$ are the range and azimuth envelope of the spectrum, respectively. β is the range frequency modulation (FM) rate. f_r and f_a are range and azimuth frequency, respectively.

3.2.2. Frequency domain focusing algorithm

To image large scenes with GEO SAR, a variety of focusing algorithms have been proposed by many scholars. Although time domain imaging algorithms (i.e., the backprojection (BP) algorithm) are universally accurate and simple, they are inefficient and thus difficult to

implement in product generation. Therefore, frequency domain imaging algorithms, most of which were based on the aforementioned high-order series range model and the analytical 2D spectrum, have been a primary focus in the study of echo focusing. The spectrum analysis algorithm has been used to quickly focus point targets within a small area [29], but it cannot be used to address the spatial variation in the scene imaging parameters at all.

In subsequent research, scholars made great efforts to cope with the key factor of the spatial variation in the scene imaging parameters. First, scholars mainly considered the range variation in the focusing parameters. In 2011, the BIT team improved the range-Doppler (RD) algorithm to suit the curve trajectory case. The algorithm is based on an adaptive adjustment of the azimuth pulse compression function parameters along the range direction [30]. However, the range variation in RCM was not considered, so the effective imaging scene size for this algorithm was limited. Since the classical chirp scaling (CS) algorithm and nonlinear CS (NCS) algorithm can be used to correct the spatial variation in RCM and have been widely applied to LEO and airborne SAR scenarios, scholars have improved these algorithms to fit the high-order range model of GEO SAR. In 2012, C. Hu from BIT [40] and M. Bao from Xidian University [41] individually proposed range CS imaging algorithms for GEO SAR. However, both algorithms can only correct range variation and are limited to first-order variation. In 2013, the BIT team proposed a range NCS algorithm for GEO SAR [39] that broadened the imaging scene width.

However, in addition to range variation, azimuthal variation also needs to be addressed for GEO SAR imaging. To address the 2D spatial variation in imaging parameters, many scholars have carried out in-depth research, most of which includes NCS operations. T. Zeng [42] and Z. Ding [43] from BIT proposed two NCS algorithms in 2013 and 2016, respectively. After range NCS are used to correct range variation in RCM, an azimuth NCS and optimal azimuth quadratic factor compensation are used respectively in the two algorithms to correct azimuthal variations in the Doppler frequencies. Quadratic factor compensation can also be used to solve the problem that the azimuth FM rates at some orbit positions are close to zero. This problem produces a very small time-bandwidth product; thus, the frequency domain azimuth matched filter is invalid. In 2015, D. Li from the National University of Defense Technology (NUDT) in China proposed an improved ωK algorithm based on azimuth NCS, where the improved Stolt interpolation and three azimuth NCSs were applied to correct the range and azimuthal variation, respectively [37]. In addition, in 2015, B. Hu from Harbin Institute of Technology proposed an improved Stolt mapping to solve the range and azimuth signals coupling problem [44].

However, the above algorithms are only suitable for the broadside mode or low squint mode cases but cannot be used for the high squint mode case. There are two possible reasons for a large squint angle, including the Earth rotation effect or beam adjustment that is done to obtain a larger coverage. The aforementioned algorithms mainly correct the azimuthal variation in Doppler coefficients because the azimuthal variation in RCM can be ignored for small squint angle cases. However, the existence of a large squint angle leads to evident range walks as well as serious azimuth-variant RCMs. To solve this problem, G. Sun from Xidian University proposed a CS imaging algorithm based on RCM equalization and subband synthesis [45] in 2014. The core approach within this method involves equalization of the azimuth-variant RCM by using high-order polynomials, and azimuth subband division and synthesis are mainly applied to compensate for the quadratic residual phase. However, grating lobes occur after subband synthesis, and the grating lobe level rises with an increasing subband number. In 2016, based on RCM equalization and range CS, J. Chen adopted two SVDs and one NCS to address the azimuthal variation in the imaging phase history [46]. In 2017, T. Zhang from BIT proposed the use of optimal azimuth polynomial compensation to weaken the azimuthal variation in RCM; then, 2D NCS can be adopted to subsequently focus the echo [47].

3.3. Main disturbance factors

GEO SAR is inevitably affected by many nonideal factors due to its long synthetic aperture time and large observation range. In 2010, D. Bruno from the Cranfield University systematically analyzed the effects of decorrelation factors on GEO SAR imaging for the first time [48]; such factors included Earth tide, ionosphere and troposphere perturbations. Including these factors will introduce phase delays to GEO SAR signals and cause the deterioration of image quality, which must be compensated to obtain high-resolution images. In addition, this team pointed out that autofocus algorithms are feasible methods for correcting ionospheric perturbation errors.

The influence of the atmosphere on GEO SAR is particularly prominent considering these factors. The most substantial difference in atmospheric influences between GEO SAR and LEO SAR is the existence of different degrees of azimuth influences caused by different levels of integration time. The frozen model can be adopted to describe atmospheric effects in LEO SAR due to its approximately 1 s level-integration time, whereas the model is invalid in GEO SAR because of a long integration time typically ranging from 100 s to 1000 s [8]. The temporally variant atmospheric effects cause image defocusing and shifting and introduce residual phase errors. The latter also severely impairs the accuracy of InSAR and D-InSAR products.

The most prominent atmospheric effects on GEO SAR imaging come from tropospheric and ionospheric perturbations. According to the variation characteristics, the troposphere can be divided into the background troposphere (slowly varying part) and tropospheric turbulence (randomly fluctuating part). Similarly, the ionosphere can be divided into the background ionosphere (slowly varying part) and ionospheric scintillation (randomly fluctuating part). Among these parts, the ionosphere and the troposphere mainly affect low band SARs (L, P, etc.) and high band SARs (e.g., Ku), respectively. It should be noted that the impacts of the atmosphere on the range imaging have little difference between LEO SAR and GEO SAR. Therefore, the study of atmospheric effects on GEO SAR mainly focuses on azimuth imaging.

3.3.1. Ionosphere effects

3.3.1.1. Background ionosphere. A phase error is introduced to the signal when electromagnetic waves pass through the ionosphere, which can be expressed as

$$\phi_{\text{ion}} = -2\pi \cdot 80.6 \cdot \text{TEC}\left(t_a\right)/(cf) \tag{3}$$

where $\text{TEC}(t_a)$ is the total electron content (TEC) in slant path at azimuth time t_a and f is the signal frequency. The presence of f denotes that the ionosphere is a dispersive medium that has different effects on different frequency signals. For LEO SAR, since the integration time is quite short, the background ionospheric effects can be regarded as temporal invariant. Therefore, only background effects on range direction need to be addressed and the split-spectrum method shows good performance if the bandwidth is large enough [20]. In 2014, L. Liang from the Institute of Electronics of the Chinese Academy of Sciences (IECAS) proposed an analysis method for considering the influence of the time-varying background ionosphere on GEO SAR and Medium-Earth-Orbit SAR azimuth imaging [49]. They expressed TEC as a Taylor expansion with respect to azimuth time and then studied the influence of the background ionosphere. These results indicated that the resolution deterioration and image shift are more significant in GEO SAR than in LEO SAR. In addition, these effects are greater with increasing integration time and signal wavelength, as shown in Fig. 3 (a) and (b).

The BIT team has conducted extensive work on the analysis of the time-varying background ionosphere [50–52]. Due to the curve trajectory and the complex observation geometry, the ionospheric effect analysis method used in LEO SAR cannot be applied to GEO SAR. In response to this problem, in 2015, the BIT team derived the 2D spectrum of the GEO SAR signal in the presence of a time-varying background ionosphere while taking the curve trajectory and long integration time into

account. The subsequent analyses showed that the effects caused by the background ionosphere, including the 2D image shift and residual phase error (causing image defocusing), were related to the derivatives of TEC and range history. The boundary conditions of the two effects were also analyzed and summarized [50]. In addition, they proposed an approach to equivalently retrieve the TEC values for the GEO SAR propagation path based on the Beidou inclined geosynchronous orbit (IGSO) navigation satellites and the Klobuchar model. The retrieved data were used to perform the GEO SAR imaging simulation in the presence of the background ionosphere, verifying the correctness of the proposed analysis method. Finally, it was found that the Phase Gradient Autofocus (PGA) algorithm performed very well in correcting the influence of the background ionosphere on a defocused area target image; see Fig. 4 (a) and (b).

In 2016, the BIT team also analyzed the impacts of the temporally and spatially variant background ionosphere on GEO InSAR and D-InSAR. The results showed that the background ionosphere produced a relative image shift and decorrelation for the InSAR pair as well as nonuniform phase screen errors for the interferogram. The inclusion of the background ionosphere can also give rise to deformation retrieval errors larger than 0.2 m, which do not satisfy the requirements for the deformation retrieval accuracy in any engineering application [53].

3.3.1.2. Ionospheric scintillation. Compared with LEO SAR, GEO SAR has a longer operation time in the area affected by ionospheric scintillation due to its much higher orbit, which makes GEO SAR more sensitive to ionospheric scintillation during the imaging process. Ionospheric scintillation also mainly affects the azimuthal-direction signal of GEO SAR.

Ionospheric scintillation is caused by the random distribution of ionospheric irregularities, introducing random amplitude and phase fluctuations into SAR echo signals. Therefore, the current methods for theoretically analyzing the ionospheric scintillation impacts on imaging are mainly based on APS theory; that is, the scintillation can be modeled as a thin phase screen. Research on the impact of ionospheric scintillation on GEO SAR has mainly been conducted at BIT and NUDT. We classify the current theoretical analysis methods into analytical methods [54–56], numerical solution methods [57], and echo simulation methods [58,59].

In 2017, the BIT team derived analytical formulas for evaluating azimuth-imaging performances of L-band GEO SAR, including PSLR, ISLR and resolution, for weak and moderate ionospheric scintillation cases. The performances were explicitly expressed as functions of the scintillation statistical indexes [54–56]. The simulation results showed that weak and moderate scintillation caused serious deterioration of the azimuth ISLR, while the azimuth resolution and PSLR deterioration could be ignored, as shown in Fig. 3 (c). In addition, in 2018, they theoretically established an interferometric phase error and decorrelation model using scintillation statistical indexes to determine the scintillation impacts on GEO D-InSAR [60].

The numerical solution methods have mainly been proposed by the NUDT team. In 2017, Y. Ji established an expression of the second moment of the GAF for GEO SAR, which can be used to evaluate the deterioration of GEO SAR azimuth resolution caused by ionospheric scintillation [57]. In addition, since the scanning velocity of the ionospheric penetration point (IPP) was much slower than that of LEO SAR, the drifting velocity of ionospheric irregularities should be considered during the analysis of GAF. The analysis results showed that the scintillation strength played a dominant role in the deterioration of the azimuth resolution, and the deterioration severity of the azimuth-imaging resolution was positively correlated to the effective velocity of the irregularities.

Regarding echo simulation methods, in 2019, the BIT team modified the power spectral density (PSD) of the scintillation phase based on the anisotropy and irregularity drifting velocity; on this basis, the SAR echoes affected by scintillation were simulated and analyzed to evaluate the performance metrics. The results showed that the image deterioration was more serious with an increasing effective velocity and angle between the satellite and geomagnetic fields [58]. In 2020, Y. Ji used the two-way ionospheric transfer function (ITF) to establish the GEO SAR echo signal model and evaluated several performance metrics, such as the resolution and interferometric coherence. The results showed that the decorrelations imposed by the anisotropic and flowing ionospheric

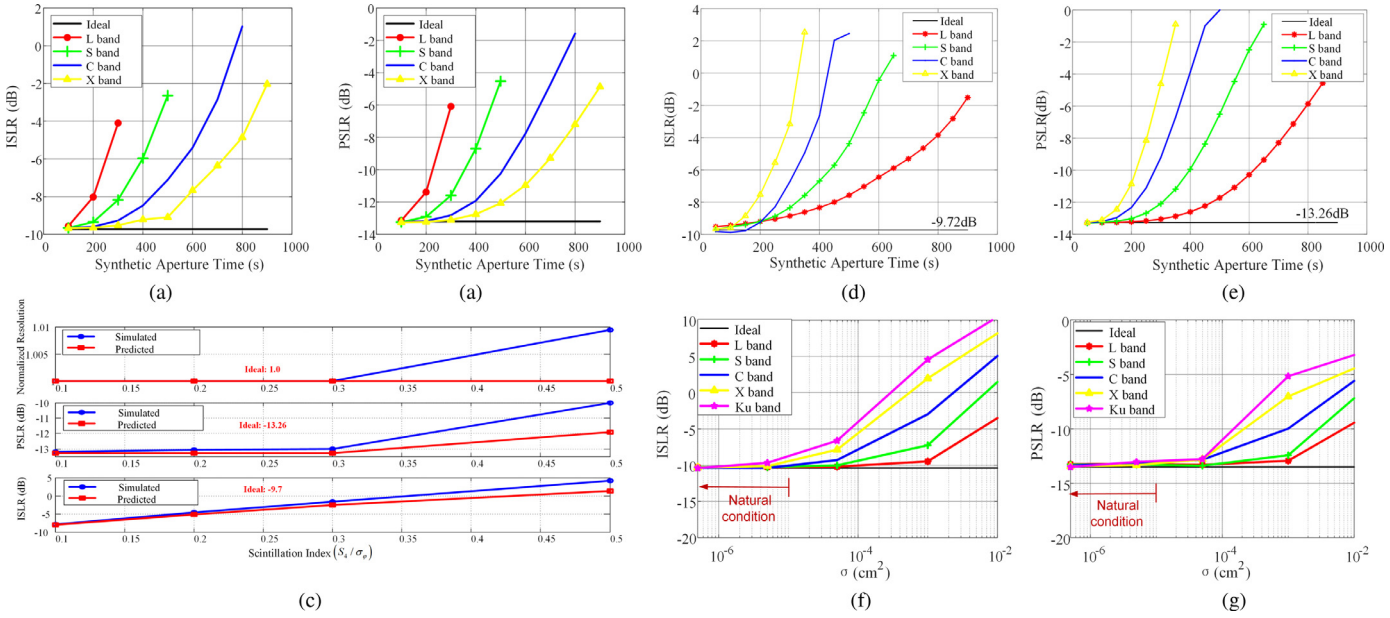

Fig. 3. Performances of GEO SAR azimuth focusing in the presence of atmospheric effects. 18° inclination GEO SAR above the equator (with a velocity of ~800 m/s) was adopted. (a) Integrated sidelobe ratio (ISLR) and (b) peak-to-sidelobe ratio (PSLR), as affected by the background ionosphere [50]. The fitting coefficients of TEC were $q_1 = 6.8 \times 10^{-3}$TECU/s, $q_2 = 7.32 \times 10^{-6}$TECU/s^2, $q_3 = 4.42 \times 10^{-12}$TECU/s^2. (c) Predicted and simulated performances in the L-band GEO SAR affected by ionospheric scintillation [54]. (d) ISLR and (e) PSLR, as affected by the background troposphere [67]. (f) ISLR and (f) PSLR affected by tropospheric turbulence, where σ is the refractive index variance [67]. An integration time of 120 s was set for (c). One can see from the simulation that the higher band GEO SAR works in, the weaker the ionospheric effects are, and the stronger the tropospheric effects are.

irregularities deeply influenced the imaging and interferometric performances of the L-band GEO SAR system [59].

In addition to the abovementioned ionospheric scintillation impact analyses, there are related works on ionospheric effect compensation. In 2016, the BIT team proposed an orbit-optimization strategy by utilizing the diurnal and geographical patterns of ionospheric scintillation occurrence to prevent GEO SAR interference from ionospheric scintillation [61]. In 2017, they also proposed an iterative method based on the entropy minimum to jointly estimate the signal amplitude and phase fluctuations and, thus, compensate for the ionospheric scintillation effects. The principle of the proposed iteration was based on the construction of a series of local quadratic fits to gradually approach the minimum entropy. The feasibility of the proposed algorithm was verified by area target simulations [62]; see Fig. 4 (c) and (d). However, the compensation method works well only for moderate or weak scintillation, and it is still challenging to remove strong ionospheric scintillation.

3.3.2. *Troposphere influences*

Research on the influence of the troposphere on spaceborne SAR can be divided into two aspects: the background troposphere and tropospheric turbulence. The background troposphere introduces time delays to GEO SAR signals, leading to additional phase errors. Tropospheric turbulence causes random fluctuations in the echo phase and amplitude, deteriorating the corresponding SAR images. Generally, the influence of the troposphere on the L-band GEO SAR is very weak [63]. Therefore, relevant studies have mainly focused on the higher bands (e.g., Ku).

In 2009, A. Monti-Guarnieri determined that the effect of atmospheric variation during observations can create a temporal-spatial variant phase shift, that is, the Atmospheric Phase Screen (APS). This APS change may give rise to azimuthal defocusing. In addition, they measured the APS variogram using ground-based (GB) SAR and indicated that the APS could be estimated and completely compensated for with a sampling time interval of 5 minutes [64].

In 2015, the BIT team deduced the analytical formula of the two-dimensional shift, azimuthal quadratic, and cubic phase errors caused by the background troposphere from the GEO SAR frequency spectrum [65]. In 2018, A. Monti-Guarnieri performed an analysis to conclude that the APS, which was mainly introduced by troposphere turbulence, caused deterioration of the resolution and interferometric correlation in

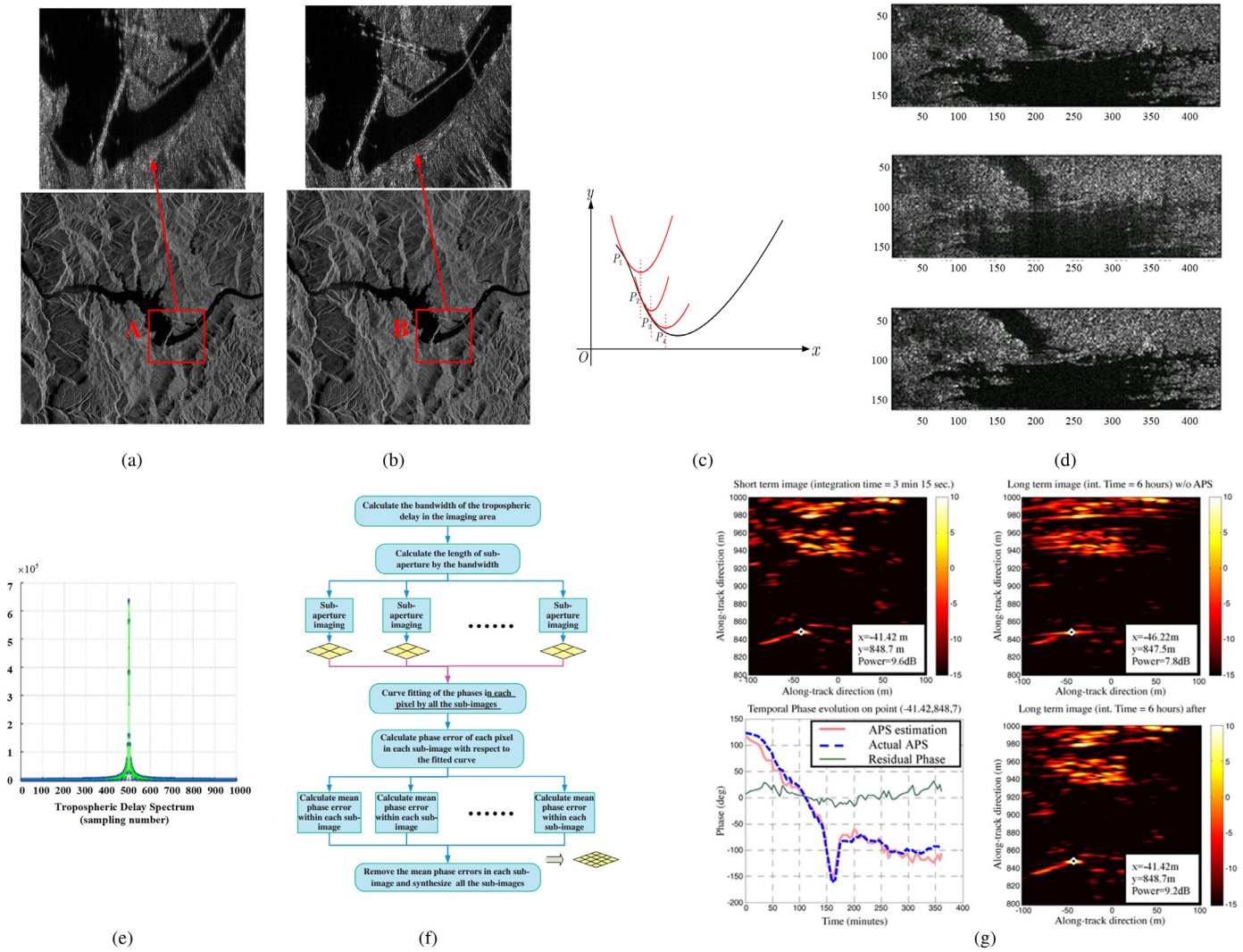

Fig. 4. Research on the compensation of atmospheric effects. SAR images in the presence of the background ionosphere (a) before and (b) after applying PGA [51]. (c) Principle of the minimum entropy algorithm that compensates for the ionospheric scintillation effects [62]. (d) Original image (top), image contaminated by the ionospheric scintillation (middle) and image after ionospheric scintillation compensation (bottom) [62]. (e) Spectrum of the measured tropospheric delay [68]. (f) Flowchart of tropospheric delay compensation based on subaperture division [68]. (g) APS retrieval and compensation experiment results based on GB SAR. (top left) Short-term acquisition, where APS was not temporally variant. (top right) Long-term acquisition without APS correction. (bottom left) APS history from long-term acquisition. (bottom right) Long-term image with APS correction [16].

GEO SAR, and an analytical expression of the interferometric correlation was established [66]. In 2019, the BIT team simulated the azimuth PSLR and ISLR affected by the background troposphere at different bands and different integration times [67]. The results showed that tropospheric phase errors caused image defocusing for the cases involving long integration times and short wavelengths, as shown in Fig. 3 (d) and (e). The effects of tropospheric turbulence were also simulated, as shown in Fig. 3 (f) and (g). These results indicated that the influence of turbulence on the L- and C-band signals could be ignored under natural conditions, while the Ku band was slightly affected by turbulence. In addition, due to the troposphere's wide distribution ranging from the ground to more than 10 km, the multiple phase screen model should be adopted for turbulence effect analysis.

In addition to the abovementioned theoretical analysis and simulation of tropospheric influences, some scholars have further studied compensation methods. In 2011, W. Sheng from the Cranfield University proposed a tropospheric delay compensation method based on the subaperture division method [68], the flowchart of which is shown in Fig. 4 (f). Analysis of the measured tropospheric delay data showed that the spectrum of the troposphere delay was concentrated in a very narrow band (see Fig. 4 (e)), so the subaperture length should be the reciprocal of the bandwidth, that is, $T_s = 1/B_t$. In this way, the tropospheric delay was almost static in each subaperture; therefore, multiple GEO SAR images with lower resolution were obtained. Then, the phases in each pixel were fitted, and the average phase error of all pixels was removed in each subimage. Finally, a high-resolution GEO SAR image was obtained.

In 2013, J. Rodon discussed a similar atmospheric phase delay retrieval method that relied on reference stable points (such as urban or rocky areas). The scattering phases of these points were stable, so their phase fluctuations could be directly interpreted as the atmospheric phase delay. They carried out a 6-hour experiment using GB SAR, and the results showed that the phase-retrieval error was within 25°. The imaging performance improved after atmospheric delay phase compensation, where the SNR loss decreased from 1.8 dB to 0.4 dB [16], as shown in Fig. 4 (g).

3.3.3. Effects of unstable targets

The long integration time of GEO SAR enables only stable targets to be fully focused, whereas unstable targets are defocused. The term unstable targets mainly refers to vegetation and other natural scenes that are easily affected by wind and may have slow motion characteristics. Since NZI GEO SAR has a particularly long integration time, research on unstable target effects has mainly been carried out by European research teams. Their studies have mainly focused on the evaluation of clutter effects on imaging. In 2006, a simulation by D. Bruno from the Cranfield University showed that unstable targets affected GEO SAR images in the form of background clutter [69]. As stated previously in the Troposphere Effects section, the analysis conducted by A. Monti-Guarnieri in 2009 indicated that the energy of the clutter expanded over a very wide area along the azimuthal direction, which introduced severe azimuth broadening, and the width was related to the time constant of the motion correlation [64]. In 2014, J. Ruiz-Rodon used the classic Billingsley model to study the SNR of GEO SAR in the presence of unstable targets and concluded that the clutter whose spectrum was located outside of the $[-1/T_s, 1/T_s]$ range was the main source of SNR worsening [70], where T_s is the integration time. However, the Billingsley model can only be applied to short integration time SAR cases, typically for integration times less than 1 s [71]. To solve this problem, in 2016, based on the Billingsley model, A. Recchia from the POLIMI derived a clutter power spectrum expression and a theoretical model for the expected signal-to-clutter ratio (SCR), and these derivations were verified by experimental data from ground-based SARs [72]. In 2019, C. Convenevole from the Cranfield University provided another model for evaluating clutter effects in the form of a physics-based clutter model. This model took reference data such as landscape statistics and weather statistics as the input, then the SCR statistics and other performance metrics (e.g., SNR) could be obtained through mathematical derivations [73]. In 2020, on the basis of the existing model, A. Monti-Guarnieri revised the decorrelation model of GEO SAR by taking the fast temporal decorrelation introduced by unstable targets into consideration. Accordingly, they proposed a novel method to evaluate the SCR and complex correlation [71]. The clutter induced by unstable targets is still an important issue having not been suppressed well.

In addition to the above factors, which attracted much attention, some other disturbance factors that affect GEO SAR imaging were also studied, including radio frequency interference [74,75] and antenna vibration [76].

3.4. InSAR/D-InSAR

InSAR and D-InSAR require further processing when repeat-pass GEO SAR images are acquired for the target region. In 2003, JPL first proposed the concept of the GESS system, which is designed for surface deformation monitoring by using inclined orbit GEO D-InSAR [23]. The research group at BIT analyzed the impact of orbit perturbation on repeated tracks of GEO SAR [28]; this study indicated that the repeated tracks formed baselines that were several kilometers to approximately 40 kilometers wide, verifying the feasibility of repeat-pass inclined GEO InSAR. This group has also conducted many studies on GEO D-InSAR applications and addressed a series of key technologies.

The main issues of inclined orbit GEO InSAR and D-InSAR are as follows: the squint-looking mode, unparallel repeated tracks, and large variations in observation angles within the full aperture. Generally, LEO SARs work under the broadside looking mode, where the line-of-sight direction is perpendicular to the flight direction. However, GEO SARs possess squint-looking geometries. As a result, the traditional LEO InSAR height-retrieval model, as shown in Fig. 5 (a), is no longer valid. To address these problems, in 2015, the BIT team deduced the general height-retrieval model for arbitrary geometric configurations by establishing an accurate slant-range vector expression. The analysis results suggested that the normal vector of the slant-range plane ($\hat{\mathbf{I}}$ in the figure) essentially determined the height-retrieval process and its performance [77], as shown in Fig. 5 (b). This new model was an extension of the LEO SAR height-retrieval model, where $\langle \hat{\mathbf{I}}, \hat{\mathbf{h}} \rangle$ and $\langle \hat{\mathbf{I}}, \mathbf{b} \rangle$ were simplified to $\sin\theta$ and perpendicular, respectively, for the LEO SAR cases.

The purpose of the data acquisition method is to select the aperture center moment (ACM) of the slave track after the ACM of the master track is determined. Due to the squint-looking geometry and the unparalleled repeated tracks in repeat-track GEO InSAR, the zero-Doppler centroid data acquisition method in LEO InSARs causes clear along-track baseline components and rotation-induced decorrelations based on spatial spectrum shifts in the interferograms. Based on wavenumber domain analysis, the researchers at BIT accurately modeled the spatial range and azimuth spectrum shifts to find the optimal data acquisition method for GEO InSAR [77]. The optimal slave SAR image can be generated according to the minimal spatial spectrum shift for the InSAR pair, minimizing the rotation-induced decorrelation and the along-track baseline component.

The large observation angle variation within the full aperture is the last issue to address to enable GEO D-InSAR applications. Compared to LEO SARs, GEO SARs can give rise to a nearly 4° viewing-angle variation between the forward- and backward-looking interferograms in MAI processing, inducing a clear geometrical distortion in the subaperture interferogram pairs, as shown in Fig. 5 (c). In the preprocessing of GEO SAR MAI, through geocoding by using external DEM data, the geometrical difference can be eliminated by coregistering the interferograms in a uniform geographic coordinate system [78]. For 3D deformation retrieval in GEO D-InSAR, the processing accuracy depends on the selection of the observation data. Therefore, we need to identify the optimal observation subapertures for the 3D deformation retrieval, as shown in Fig. 5 (d). To effectively evaluate the 3D deformation measurement ac-

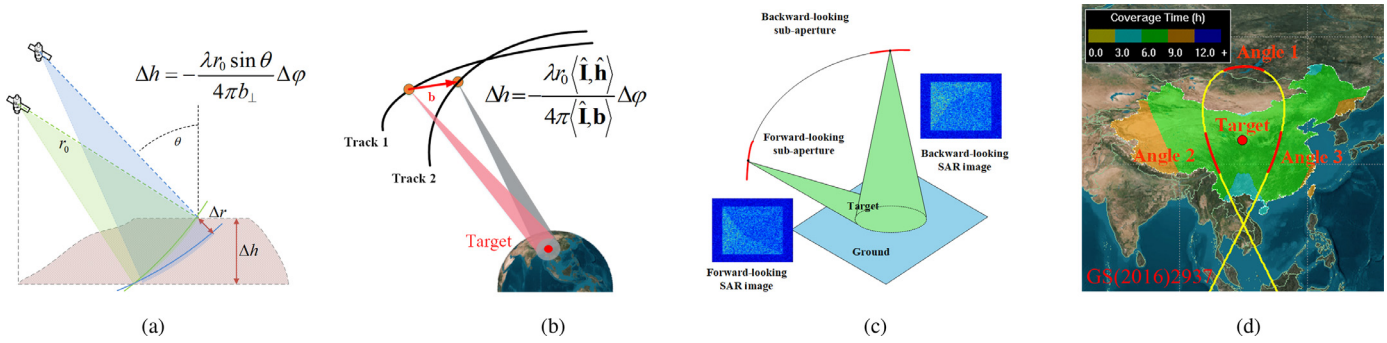

Fig. 5. Main GEO InSAR/D-InSAR processing issues. (a) Height-retrieval model in LEO InSAR, where Δh is the height of target to be retrieved, λ is the wavelength, r_0 is the slant range, θ is the incident angle, $b_\perp$ is the perpendicular baseline, and $\Delta\varphi$ is the phase difference induced by slant range Δr difference between the two observations. (b) Height-retrieval model in GEO InSAR [71]. $\hat{\mathbf{l}}$ is the elevation direction, $\hat{\mathbf{h}}$ is the altitude direction, and $\mathbf{b}$ is the baseline vector. (c) Geometrical difference between the forward- and backward-looking SAR images [78]. (d) Selection of multiple subapertures in GEO SAR 3D deformation retrieval.

curacy under various geometric configurations, the BIT team introduced the concept of geometric dilution of precision (GDOP), which is a typical indicator used in navigation satellite system applications [24]. The basic approach for this concept was to acquire the east-west, north-south, and height components of the deformation individually and then to calculate the root mean square (RMS) error as the overall accuracy. The accuracy is proportional to the position dilution of precision (PDOP); thus, when the PDOP is minimized, the best geometric combination of the observation data is obtained.

3.5. Equivalent experiment

Since there are no in-orbit GEO SARs, it is difficult to directly verify the above theoretical research on GEO SARs. Considering the orbit characteristics and the observation geometry of GEO SAR, scholars have proposed various types of equivalent experiments. Since the NZI GEO SAR motion characteristics studied by European scholars are relatively simple, the extremely long integration time is the main concern when designing a verification experiment. At present, such experiments mostly employ the scheme of long-term ground-based SAR imaging to verify the relevant theoretical analyses, including APS retrieval and compensation [16]. The inclined GEO SAR satellite studied by Chinese scholars has a complex trajectory and observation geometry. Therefore, in addition to the long integration time, the characteristics of orbit and Doppler frequency should also be considered in verification experiments. Considering the many similarities between the inclined GEO SAR satellites with large "figure 8"-shaped nadir-point tracks and China's Beidou inclined geosynchronous orbit, IGSO, navigation satellites, the BIT team conducted several equivalent experiments based on the Beidou IGSO satellites [79], which will be described herein.

3.5.1. Experimental principle

The similarities between the inclined GEO SARs and the Beidou IGSO satellites mainly lie in their orbits and payload parameters. Some similarities and equivalences are summarized as follows. (a) These systems have similar orbits. In particular, their inclinations are very close, inducing similar effective velocities. (b) Their carrier frequencies (L-band) and bandwidths (~ 20 MHz) are almost the same. (c) Both of these systems can be used to provide long illumination times and have curved satellite trajectories, which are the basic characteristics of inclined GEO SARs. (d) The signals of both these systems pass through and are affected by the atmosphere. Some key parameters of the inclined GEO SARs and Beidou IGSO satellites are listed in Table 1. Their nadir points are shown in Fig. 6 (a).

Based on the above equivalence analysis, the BIT team designed the GEO SAR equivalent verification experiment based on the Beidou IGSO satellites. Note that GEO SAR and Beidou IGSO are different in some aspects. One important difference is that the GEO SAR transmits linear frequency modulation signals while the Beidou IGSO satellite transmits pseudo-random code. Therefore, complex preprocessing based on global navigation satellite system (GNSS) is necessary before echo focusing. The experimental geometries are shown in Fig. 6 (b) and (c). An echo antenna was used to receive the backscattered echo signal reflected from the illuminated target area. Since bistatic SAR geometry is adopted, a direct signal antenna, which directly received the Beidou IGSO satellite signal for phase synchronization and range pulse compression, was set near the echo antenna. These two antennas were placed on the top of a tall building to reduce the effect of or prevent other buildings from shielding the signals. The imaging time and the time intervals were determined according to the experimental goal, performance requirements and ephemeris of Beidou IGSO satellites.

Table 1
Comparison between the key parameters of the GEO SAR and Beidou IGSO satellites [72].

parameter	GEO SAR	Beidou IGSO_2
Semimajor axis (km)	42164	42162
Inclination (°)	53	53.4
Eccentricity	0	0.005
Band	L	L
Bandwidth (MHz)	18	~20

The equipment use for this experiment is shown in Fig. 6 (d)-(f). After phase synchronization and range pulse compression aided by the direct signal, the additional phase that was inherently induced by the bistatic geometry (e.g., the range from the satellite to the direct antenna and the range from the target to the echo antenna) was compensated. Next, SAR images could be formed by the BP algorithm.

3.5.2. Experimental results

Three equivalent experiments for GEO SAR were carried out by the above experimental schemes: an imaging experiment, a 3D deformation retrieval experiment, and a TomoSAR experiment.

3.5.2.1. Imaging experiment. This experiment was carried out on the Changshu campus of BIT in July 2013 [79], with the goal of verifying the feasibility of long integration time imaging by GEO SAR. The experiment geometry is shown as Fig. 6 (b). There was a lake, a factory, a toll station, roads, and other targets in the illuminated scene, and a transponder was set up to conveniently evaluate the resulting 2D resolutions. The integration time was set as 1800 s. According to the method presented in [29], the theoretical range and azimuth resolution were 17.77 m and 1.73 m, respectively. The focusing result is shown in Fig. 7 (a), as measured from a point target (i.e., the transponder); the corresponding experimental resolutions in the two directions were 19.09 m and 1.75 m, with errors of 7.5% and 0.65%, respectively. These

results verified the proposed GEO SAR resolution analysis method [29]. In addition, the imaging results were highly consistent with the optical image provided by Google Earth, i.e., the outlines and locations of many elements in the scene, such as the factory, toll station and roads, overlapped very well in the two images, as shown in Fig. 7 (b). This experiment verified the feasibility of long integration time imaging by GEO SAR and showed that GEO SAR had great application prospects in remote sensing.

3.5.2.2. Experimental results for 3D deformation retrieval. This experiment was carried out at BIT in May and June 2016 [80] to verify the theoretical performance analyses of the multiangle 3D deformation retrieval of GEO SAR. The experimental geometry is shown in Fig. 6 (c). Two direct antennas were used in the experiment, of which one was used for synchronization and range pulse compression; the position of the other antenna (called the deformation antenna, set as the observed target) was artificially and precisely controlled by high-precision displacement equipment. Then, the signal from the deformation antenna was amplified by a transponder and transmitted to an echo antenna next to the first direct antenna. In this experiment, 16 data sets were collected, corresponding 16 days, where each data set consisted of data from IGSO 1, 2, 4, and 5. The displacement of the displacement device were set to be 2 cm and 1 cm for the second day and final two days. 900 s of data were collected to form an image. The imaging results of the transponder are shown in Fig. 8 (a)-(d). Taking the position of the deformation antenna on the first day as the reference, the positions of the deformation antenna on each day are shown in Fig. 8 (e), where one can see only the deformation in the altitude direction (i.e., Z direction) was fixed. Fig. 8 (f) shows the retrieved and reference deformations, from which the retrieval accuracy (i.e., relative motion equation (RME) of error) in the X, Y and Z directions can be evaluated as 1.68 mm, 2.82 mm and 4.22 mm, respectively. This experiment showed that GEO SAR can be used to realize 3D deformation retrieval with an accuracy on the millimeter level, which is of great significance to dynamic detection in urban areas and disaster reduction/prevention in natural areas.

3.5.2.3. TomoSAR experimental results. This experiment was conducted at BIT in March 2016 [81]. The experimental geometry is shown in Fig. 6 (e). A total of 23 repeat-track echo data sets were collected within one month. The perpendicular baseline span in the experimental period, generated by the satellite's repeat tracks, was approximately 430 km (see Fig. 9 (a)), corresponding to a theoretical Rayleigh resolution of ca. 5 m in the altitude direction. The integration time for each SAR image was 900 s. After 2D SAR echo data focusing for each track, SAR images with a signal-to-noise ratio of about 15 dB, were formed. Then, two points, A and B, with stable and high backscatter intensities were selected for tomography processing along the elevation direction. Then, the profiles of these two points along the azimuthal direction were presented and served as examples for performance evaluation. The tomographic profiles are shown in Fig. 9 (b), where points A and B correspond to two tall buildings. To verify the tomography results, LiDAR was used to obtain the point cloud data of the imaged scene (see Fig. 9 (c)), from which high-precision digital elevation model data of A and B were extracted, and then the tomography results were compared to the high-accuracy data. The results showed that in the IGSO tomography data, the height errors of the two buildings were 2.2 m and 3.4 m, respectively, verifying the feasibility of GEO SAR tomography.

4. Multiplatform GEO SAR

As monostatic GEO SAR has been studied in detail, scholars have gradually realized its limitations regarding some mission performances or signal processing, such as the infeasibility of global coverage and difficulty of compensating for the atmospheric impact under its long integration time. Some of the above shortcomings can be overcome by introducing additional platform(s), forming a multiplatform GEO SAR

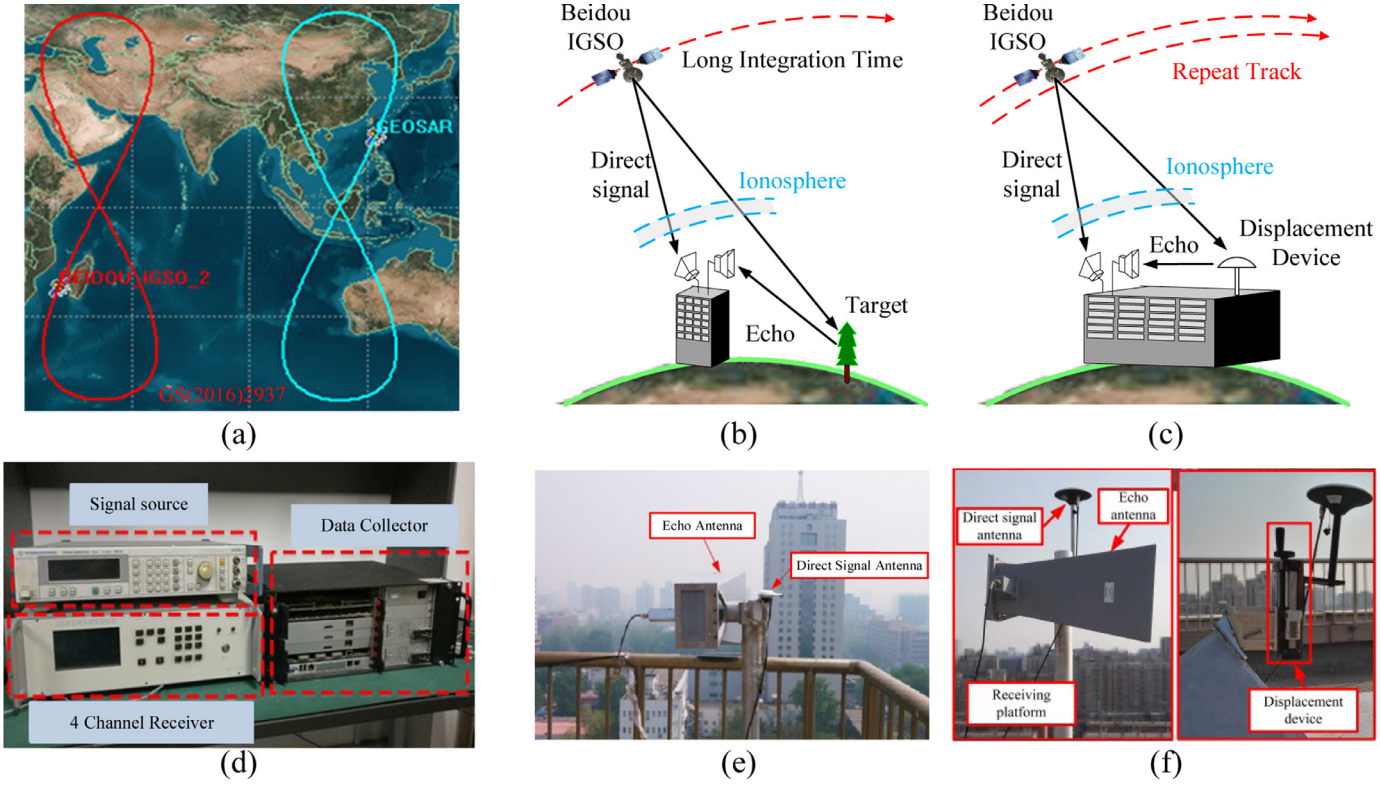

Fig. 6. GEO SAR equivalent verification experiment based on the Beidou IGSO satellite. (a) Nadir points of the inclined GEO SAR and Beidou IGSO satellites. (b) Geometry adopted for the SAR imaging experiment and TomoSAR experiment. (c) Geometry adopted for the 3D deformation retrieval experiment. (d) Data-collection equipment. (e) Antennas adopted for the SAR imaging experiment and TomoSAR experiment. (f) Antennas adopted for the 3D deformation retrieval experiment.

system. Moreover, the wide coverage of monostatic GEO SAR also facilitates research on some new multiplatform GEO SARs. Therefore, in addition to monostatic GEO SAR, research on multiplatform GEO SAR is also ongoing. The multiplatform GEO SAR discussed herein mainly includes a GEO SAR constellation, GEO-LEO/airborne/unmanned aerial vehicle bistatic SAR, GEO SAR exploiting formation flying (FF-GEO SAR), etc.

4.1. GEO SAR constellation

A GEO SAR constellation is a multisatellite system composed of several independent monostatic GEO SARs; its main function is to improve the coverage performance of GEO SAR so that it can cover most regions of the world. The first GEO SAR constellation concept was the GESS proposed by JPL in 2003 [23], in which 10 highly inclined GEO SAR satellites were divided into five groups and uniformly dispersed along the Earth's longitude to cover the world, as shown in Fig. 10 (a). Each group contained two satellites with a phase difference of 180°, resulting in an interferometric repeat time of 12 hours. The main task of the constellation was to achieve 3D deformation measurements within accuracy ranges of a few millimeters in 24-36 hours to predict earthquakes on a global scale. In 2006, S. Hobbs proposed a GEO SAR constellation consisting of 12 receiving-only satellites operating in NZI geosynchronous orbits. Broadcast satellites were considered as the signal sources [12]. The 12 satellites were divided into three groups, which were distributed over the American, African and Asian continents, to cover most of the land on Earth (see Fig. 10 (b) for the beam coverage areas). Four satellites in each group operated in two pairs of concentric circles, where the satellites in the outer circles performed the main task of Earth observation, and the satellites in the inner circles were used to eliminate part of the sidelobe energy and thus to improve the SNR. In 2019, H. Xu from the University of Chinese Academy of Sciences raised a GEO SAR constellation composed of 5 180°-inclination GEO SARs evenly distributed along the longitudinal direction. This 180° inclination meant that every satellite ran in a reverse-equatorial geosynchronous orbit, opposite to the Earth's rotation direction, making each satellite's effective velocity twice its inertial velocity and more than 6 km/s. Through the beam switching of each satellite, continuous observations were realized in the middle-latitude area [82], as shown in Fig. 10 (c).

4.2. GEO-LEO/airborne/unmanned aerial vehicle (UAV) bistatic SAR

As early as 1997, the MITRE Corporation in the U.S.A. investigated GEO-UAV bistatic SAR moving target indication (MTI) applications [83]; they pointed out that an array antenna could be employed as the receiver for airborne MTI or ground MTI. In 2010, the U.S. Navy studied the application of GEO spaceborne-airborne bistatic SAR (SA-BSAR) in target tracking and fire control, and the system design, tracking scheme and firing computation were discussed [84]. Other research has mainly focused on GEO SA-BSAR and has mostly been conducted by Chinese scholars. Since 2015, scholars from the University of Electronic Science and Technology of China (UESTC) have carried out extensive research on system design and imaging algorithms. At present, GEO SA-BSAR research mainly focuses on system design, imaging algorithms, and moving-target detection.

Regarding system design, in 2010, J. Zheng from the Institute of Electronics of Chinese Academy of Sciences proposed that the installation of multiple channels along the range direction in an airborne receiver would induce a spectrum offset between channels, and the range resolution could be improved through spectrum synthesis [85]. In 2016, Z Sun from the UESTC demonstrated that GEO SA-BSAR can be used to provide higher spatial resolution and SNR than monostatic GEO SAR [86]. Other advantages of GEO SA-BSAR included low system complexity, low power consumption, and high flexibility in the motion parameter adjustment for imaging performance optimization. The motion parameters can be optimized through multidimensional function optimization with a genetic algorithm. For GEO-UAV bistatic SAR, to ensure UAV safety, 3D path planning can be carried out to achieve optimal imaging performance [87].

Regarding imaging algorithms, in 2007, Y. Yuan from Beihang University pointed out that the Doppler history was azimuth-variant in the GEO SA-BSAR system. To solve this problem, they improved the classical RD algorithm by dividing the echo data in the azimuthal direction [88]. Time and frequency synchronization were realized by means of direct waves [89]. Other research on GEO SA-BSAR imaging was primarily carried out by the UESTC team. They mainly studied a system with a multichannel airborne receiver, where the channels were assumed to be along the flying direction to solve the Doppler aliasing problem that resulted from the much lower PRF of GEO SAR compared to the Doppler bandwidth of the echo. In 2018, J. Wu used the multichannel transfer function to reconstruct the spectrum. The reconstruction performance can be assessed based on the azimuth ambiguity-to-signal ratio (AASR), and the optimal array design can be obtained by minimizing this AASR [90]. In addition, the transfer function can be used as a weighting coefficient to focus the GEO SA-BSAR echo by a fast factorized BP algorithm [91], whose principle is shown in Fig. 11 (b); corresponding simulated images before and after spectrum reconstruction are shown in Fig. 11 (c) and (d), respectively. In 2019, H. An verified that NCS processing can be used to equalize the 2D space-variant Doppler centroid, which narrowed the Doppler bandwidth and reduced the channel number [92]. In 2020, the analysis by Z. Sun showed that the two-way range history was equivalent to that of a bistatic SAR with a fixed transmitter, and then

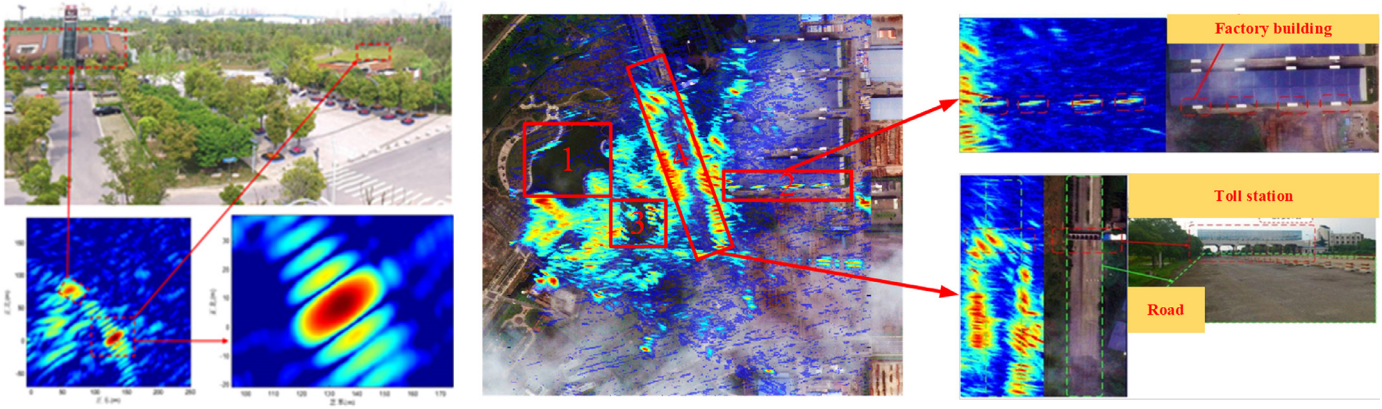

Fig. 7. Imaging experiment results based on the Beidou IGSO satellite. (a) Focusing result from the transponder. (b) Focused area targets, compared to optical images.

the echo can be isolated using a 2D Stolt transformation [93], obtaining better imaging results than the NCS-based algorithm [92].

Regarding moving-target detection, in 2009, H. Shi from the Beihang University pointed out that azimuth multichannel and fractional Fourier transform techniques can be applied to suppress clutter and realize the detection and parameter estimation for slowly moving ground targets [94]. In 2020, X. Dong form BIT raised a GEO SA-BSAR configuration design method for moving target detection (MTD) applications [95]. The key idea was to determine the relationship between the performances (both MTD and SAR resolution) and the configuration parameters of the receiver. Then, these parameters were optimized and output. In view of the inevitable spectrum aliasing problem of moving targets, Y. Zhang from BIT proposed the realization of spatial filtering by using 24 channels [96]. In this method, a large number of channels can be used to offer enough spatial samplings, making each sampling of the aliased spectrum in the wavenumber domain approximate to a single-frequency signal. Therefore, the spectrum of each channel can be extracted separately and then spliced into a full spectrum. W. Xu from Inner Mongolia University of Technology pointed out that Doppler aliasing could be mitigated by azimuth NCS, and then the targets' radial velocity could be estimated by maximizing the signal-to-interference ratio [97]. H. An determined that the imaging problem of moving and stationary targets could be modeled as a joint optimization problem, which aimed at optimizing the entropy of the moving-target image and the residual error of the final image at the same time. In this way, both stationary and moving targets can be focused, and even the number of channels required for resolving ambiguity can be reduced [98].

4.3. FF-GEO SAR

FF-GEO SAR employs multiple GEO SARs flying in formation to simultaneously observe the Earth. Satellites in an FF-GEO SAR work cooperatively, and their echoes or images need to be processed coherently. There are various tasks and configurations related to FF-GEO SAR, and they are intended to improve the performance of monostatic GEO SAR.

4.3.1. FF-GEO SAR concepts

In 2012, A. M. Guarnieri proposed the concept of geosynchronous earth monitoring by interferometry and imaging (GEMINI). The key idea was based on the employment of one or more pairs of near-spaced twin GEO receivers to collect signals from a common SAR sensor (see Fig. 10 (d)). An image pair with an interval of a few minutes was formed to generate a temporal decorrelation-free interferogram for applications including weather prediction, landslide monitoring, etc. [99]. In 2015, because the extremely long integration time in NZI GEO SAR could result in decorrelation due to the uncompensated APS, A. M. Guarnieri proposed the concept of the Advanced Radar Geosynchronous Observation System (ARGOS) [100, 101], which was composed of N transmitting-and-receiving satellites and M receiving-only satellites, forming $N_{\mathrm{TOT}} = N(N+1)/2 + MN$ equivalent phase centers, as shown in Fig. 10 (e). In theory, if these phase centers were evenly distributed, the 8-hour integration time of monostatic GEO SAR could be shortened to $1/N_{\mathrm{TOT}}$ of the original integration time, i.e., 35 minutes. This system can effectively alleviate the influences of the APS effect and the internal motion clutter on the images.

4.3.2. Research on FF-GEO SAR

Based on the Major International (Regional) Joint Research Project funded by the National Natural Science Foundation of China, the BIT team, the Cranfield University team, and the POLIMI team are cooperatively carrying out research on FF-GEO SAR. The plans for this project include adding several passively receiving satellites to the currently demonstrated monostatic GEO SAR with a small "figure 8"-shaped nadir-point track. The system configuration consists of two formations, a closely-spaced formation (GEO1 and GEO2) and a far-spaced formation (GEO1 and GEO3), as shown in Fig. 12 (a). The two satellites in the near-spaced formation form real-time baselines for the TomoSAR mission (see Fig. 12 (b)), while GEO3 can be used to expand the observation angles (especially in the east-west direction) of the master satellite, improving the 3D deformation retrieval accuracy (see Fig. 12 (c)).

We consider the key issues of this FF-GEO SAR system as follows. (a) Formation design. Designing the orbital elements of the two master satellites to optimize the mission performances in theory is a prerequisite. (b) Bistatic imaging. Bistatic SAR mode is adopted in the system (GEO1-GEO2, GEO1-GEO3), so it is necessary to study efficient frequency domain focusing algorithms, for which the large bistatic angle in GEO1-GEO3 (initially estimated to be up to 30°) and the squint mode need to be addressed. The phase and frequency synchronization scheme must also be considered. (c) Multiangle 3D deformation retrieval. The 3D deformation retrieval performance is closely related to the combination of observation angles. One of the angles in FF-GEO SAR is supplied by GEO1-GEO3, which means it is a large bistatic angle. Nevertheless,

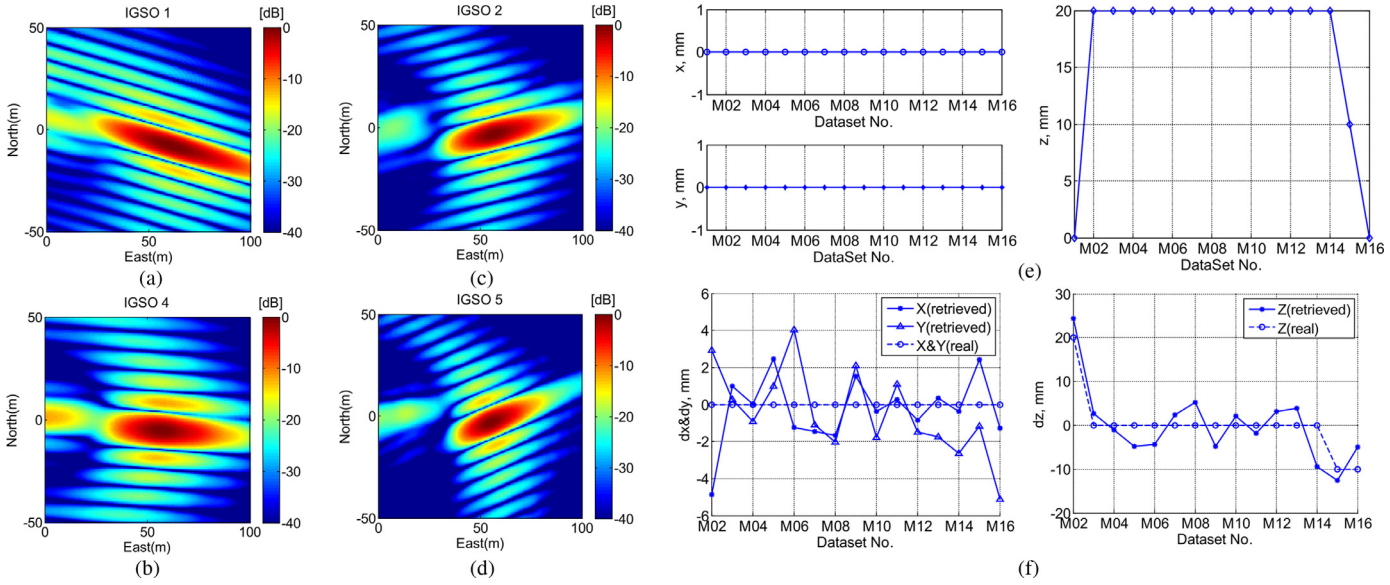

Fig. 8. Experimental results of 3D deformation retrieval [80]. (a)-(d) Experimental images from the transponder. (e) Artificial position history of the deformation antenna. (f) Estimated deformations in all directions.

Table 2
Orbital elements of the master satellite and the designed slave satellites.

Orbital Elements	Value		
	Master (GEO1)	Slave 1 (GEO2)	Slave 2 (GEO3)
Semimajor axis (km)	42164	42162.914	42164
Inclination (°)	16	16	16
AoP (°)	0	-0.0243	0
Eccentricity	0	0	0
LAN (°)	90	90.0383	129.8
True anomaly (°)	0	0	0

there are few studies on deformation retrieval in large bistatic angle cases. Therefore, it is necessary to study optimal angle selection in the presence of a large bistatic angle. (d) TomoSAR affected by complex baselines. Compared to traditional LEO TomoSAR, both the repeat-track baselines and formation baselines of inclined GEO SAR are clearly non-parallel. Therefore, it is necessary to study TomoSAR performance analysis and signal processing methods under complex baselines. We will discuss some recent research progress on multiangle 3D deformation retrieval and TomoSAR.

4.3.2.1. 3D deformation retrieval. The 3D deformation retrieval mission is conducted by the far-spaced formation. Recently, we designed this formation and analyzed its deformation retrieval performance. To increase the observation angle difference in the east-west direction, we considered setting GEO3 to have the same shape of subsatellite track as the master satellite, but the two were spaced very far apart along the longitudinal direction, i.e., the only orbital element difference between the two was the longitude of the ascending node (LAN). At least three observation angles are required to realize 3D deformation retrieval, and the optimal LAN of GEO3 can be determined at the point when the 3D deformation retrieval is the most accurate, i.e., when the corresponding PDOP is the minimum. Assuming that $\mathbf{S}_1$ and $\mathbf{S}_2$ are in the track of GEO1 and $\mathbf{S}_3$ is in the track of GEO3, the center of China (point P_0 in Fig. 13 (a)) was selected PDOP evaluation. For a certain LAN of GEO3, we extensively searched $\mathbf{S}_i (i = 1, 2, 3)$ and found the optimal PDOP value (which was locally optimized). Each LAN will output a single local optimal PDOP, so by dividing the LAN range into sufficient grids and comparing all the locally optimal PDOP values for all LANs, we finally obtained the globally optimal PDOP (which is minimal), and the corresponding LAN was the desired parameter. On the other hand, if the LAN difference between GEO1 and GEO3 is too large, some regions of China cannot be observed at an effective incidence angle (10°~60° is assumed here). Therefore, during the LAN optimization, we restricted all the edge points in China (dots in Fig. 13 (a)) to be effectively observed by GEO3 in one or more orbit positions. To obtain good coverage for China, the master satellite's orbital elements are set as GEO1 listed in Table 2. the designed orbital elements of GEO3 are shown in Table 2. The theoretical optimal deformation retrieval accuracies were evaluated for some cities in China and are shown in Fig. 13 (b)-(d). The deformation measurement performances of FF-GEO SAR in the three directions are similar and all measurement performances are on a scale of 1 cm. The results show that the retrieval accuracy in the east-west direction is the best in FF-GEO SAR, successively followed by the large "figure 8" and small "figure 8" (GEO1 was employed for simulation) monostatic GEO SAR. Compared with the case involving only the master satellite, the retrieval accuracy in the east-west direction was improved by an order of magnitude using FF-GEO SAR.

4.3.2.2. TomoSAR. Affected by orbit perturbation, the repeat tracks of monostatic GEO SAR will drift within days [81], forming perpendicular baselines for the TomoSAR mission. The perturbation causes this drift by changing the orbital elements of the satellite. Therefore, by artificially adjusting the semimajor axis (denoted as a) of GEO SAR, eastward (a>42164 km) or westward (a<42164 km) drift of the repeat track can also be induced [102].

Inspired by this, we presented an idea of TomoSAR realization using the near-spaced GEO SAR formation. The basic design involves the introduction of the orbital element differences between the master satellite GEO1 and slave satellite (GEO2) so that the two satellites have different drifting speeds of the repeat tracks, and then the intersatellite baseline varies with days.

In terms of TomoSAR, the main difference between monostatic GEO SAR and FF-GEO SAR is that the former directly employs single-look complex (SLC) images, while the latter first constructs a single-pass interferogram stack from the image pairs obtained every day, and then, the stack of interferograms is adopted for tomography. The latter is called coherence-based TomoSAR [103]. The primary advantage of FF-GEO coherence-based TomoSAR is that it mitigates the temporal decorrelation due to the pair of images that are collected nearly simultaneously every day [103]. In addition, this method can be used to greatly shorten the total time span required for data collection compared with LEO SAR (1/11 of the LEO SAR, taking TanDEM-X as an example, whose revisit time is 11 days). These advantages decrease the data impact due to the structural changes in the scene, such as variations in tree canopies and deformations of urban areas.

To realize FF-GEO coherence-based TomoSAR, it is necessary to design the orbital elements of the slave satellite GEO2. The RME, which describes the motion of the slave satellite relative to the master satellite in the Earth-centered inertial (ECI) frame, can be used to calculate intersatellite baselines and has become the main principle for designing of GEO SAR formations. Nevertheless, the inertial velocity and effective velocity of GEO SAR are significantly different due to Earth rotation effects. Therefore, it is more accurate to adopt the RME in the Earth-centered-Earth-fixed frame (ECF) [25] to express these intersatellite baselines, including the along-track baseline $\tilde{y}(t)$ and the perpendicular baseline $\tilde{z}(t)$ [25].

The following two constraints need to be considered in the design of FF-GEO coherence-based TomoSAR. (a) The perpendicular baseline

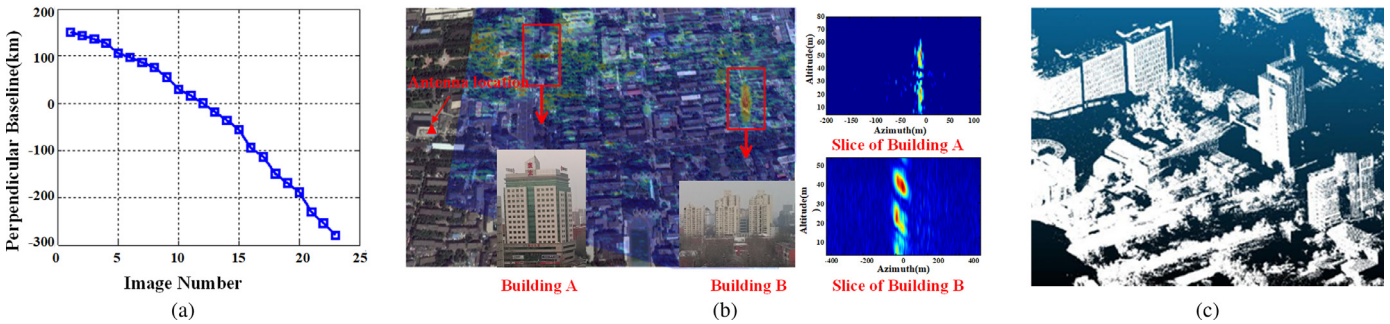

Fig. 9. TomoSAR experimental results [81]. (a) Perpendicular baseline. (b) 2D and tomography results for buildings A and B. (c) Point cloud data of the imaged scene.

should change linearly with days, while also changing in accordance with the initial value B_0 and the interval ΔB given previously. (b) The along-track baseline should be as small as possible to improve the correlation coefficient (CC) of each single-pass image pair. To meet constraint (a), it is necessary for the master and slave satellites to have slightly different semimajor axes. In GEO SAR, $\tilde{z}(t)$ and $\tilde{y}(t)$ are time-varying and, because of the semimajor axis difference, are both aperiodic functions. Therefore, the RMS value of baselines are considered instead of the instantaneous values, and the optimization problem of formation design can be constructed as

$$\begin{aligned} \min \quad & \sqrt{\sum_{k=1}^{K}\frac{1}{KT}\int_0^T \tilde{y}^2(k\cdot T+t)dt} \\ s.t. \quad & \sqrt{\sum_{k=1}^{K}\frac{1}{KT}\int_0^T [\Delta\tilde{z}(k\cdot T+t)]^2 dt} = |\Delta B| \\ & \sqrt{\frac{1}{T}\int_0^T \tilde{z}^2(t)dt} = |B_0| \end{aligned} \tag{4}$$

where T is the orbital period and K is the total number of days for tomographic data collection. Assuming $K = 10$ and $B_0 = \Delta B = 9.5$ km, the designed orbital elements of GEO2 according to the parameters of GEO1 are shown in Table 2. The perpendicular baselines at each AoL are shown in Fig. 14 (b). In most orbit positions (AoL = 0 ~ 80° out of the AoL = 0 ~ 90° range), the perpendicular baselines have good linearity over time. Moreover, the error of the perpendicular baseline is less than 8% of the design requirements for 83.3% of the positions on the whole track, as shown in Fig. 14 (c). More specific work is still underway.

Another problem of FF-GEO coherence-based TomoSAR is that the baseline span can be very large. Since the intersatellite baseline varies linearly with the number of days, the baseline can approach or even exceed the critical baseline. The implementation of a large baseline can improve the elevation Rayleigh resolution for SAR tomography, but the CC of the image pairs correspondingly decreases. However, currently, neither SLC-based TomoSAR nor coherence-based TomoSAR processing has taken this CC decrease into account. The traditional compressive sensing method for coherence-based TomoSAR is expressed on the left of Fig. 14 (e), where g_m is the m-th image, $\mathbf{A}$ is the mapping function, and ϵ is the threshold related to the noise level. We found that based on the maximum likelihood criterion, weighting coefficients derived from CC can be applied to improve the CS-based method. The improved algorithm is shown on the right of Fig. 14 (e), where $\Gamma_{m,n} = \gamma(g_m, g_n)$ represents the CC between images g_m and g_n. To verify this improved algorithm, we constructed a scene consisting of a pyramid, as shown in Fig. 14 (d). The wavelength was 24 cm, the bandwidth was 18 MHz, the scene pixel spacing was 10 m, and the pyramid height was 80 m. The scene size and the pyramid size were 200 pixels × 200 pixels and 160 pixels × 160 pixels, respectively. Based on the parameters in Table 2, the satellites' tracks from the 12th to 14th day were utilized to generate and focus the echoes. Finally, the 100th range bin was selected for tomography, and the corresponding results are shown in Fig. 14 (f) and (g); the accuracies were estimated to be 2.46 m and 1.20 m for the traditional and improved methods, respectively, suggesting a 51% improvement. The simulation verified the effectiveness of the improved algorithm. More specific work is currently underway.

5. Conclusion and perspective

This article reviews the main research progress regarding GEO SAR. The main orbit schemes, including NZI and inclined GEO SAR, are described. To form images of high qualities, key technologies, including system design, echo focusing, disturbance factors, should be addressed. The complex geometry of repeat tracks and a large squint angle cause the classical deformation retrieval methods in LEO SAR to be invalid in GEO InSAR and D-InSAR.

The aforementioned challenges have been studied in depth and many novel solutions have been proposed. The influence of the Earth's rotation on system design, including resolution analysis and beam steering, has been modeled. Based on the high-order polynomial range model

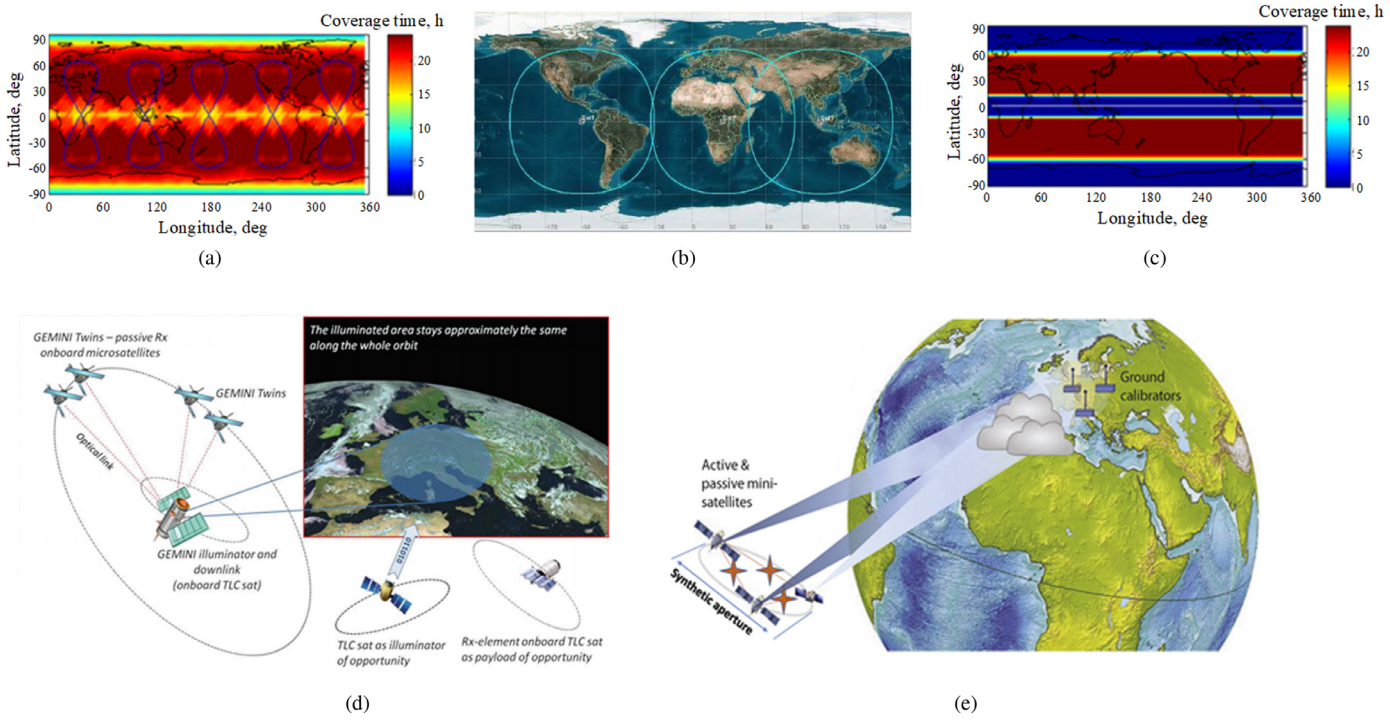

Fig. 10. GEO SAR constellation and formation concepts. (a) The GESS for global earthquake prediction [18]. (b) The constellation proposed by a team at Cranfield University [12]. (c) A constellation with SARs flying in a reverse-equatorial geosynchronous orbit [82]. (d) The GEMINI concept for the realization of single-pass InSAR missions through twin receivers [99]. (e) The ARGOS concept, a MIMO system for integration reduction by means of multiple phase centers dispersed along the whole aperture [100].

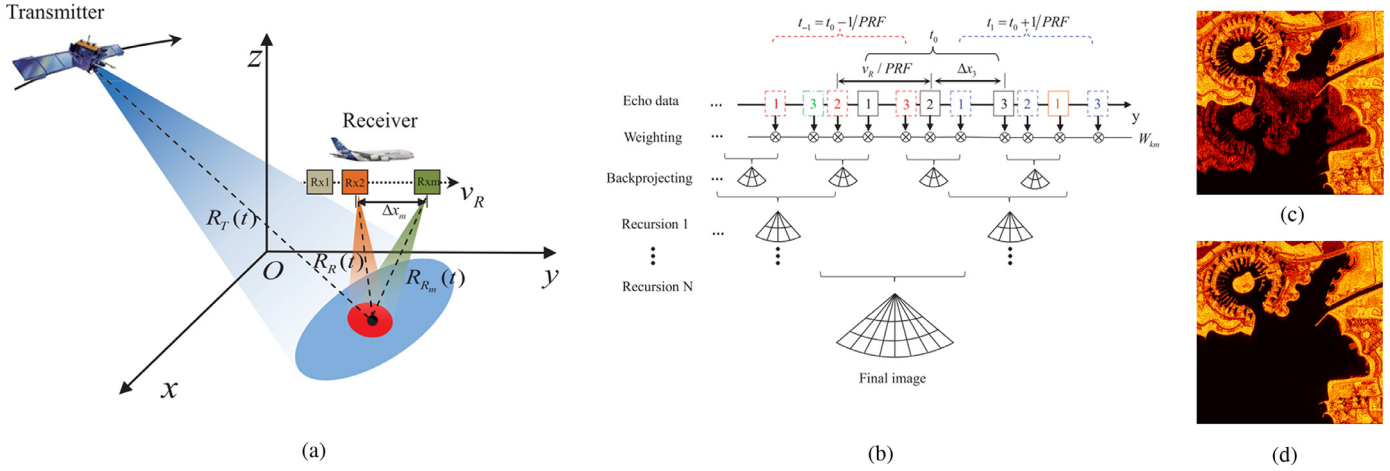

Fig. 11. Examples of GEO SA-BSAR studies [91]. (a) System configuration. (b) A fast factorized BP algorithm. Images (c) before and (d) after Doppler ambiguity suppression.

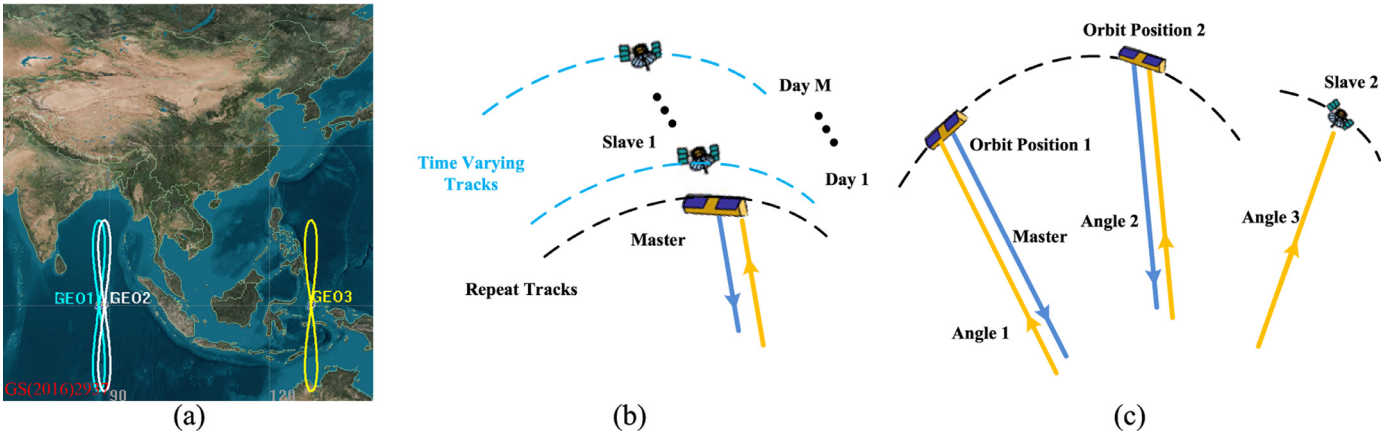

Fig. 12. FF-GEO SAR based on medium-inclination GEO SAR. (a) Orbit configurations, where GEO1 is the master satellite, GEO2 and GEO3 are the receiving-only slave satellites. (b) Coherence-based mission conducted by GEO1 and GEO2. Intersatellite baselines can be constructed based on the subsatellite track shift of GEO2 relative to GEO1. (c) 3D deformation retrieval mission conducted by GEO1 and GEO3. Two observation angles and final angles are provided for GEO1 and GEO3, respectively.

and the frequency domain imaging algorithms with NCS as the basic steps, the high phase-preserved echo focusing of large scenes has been basically addressed. Through Taylor expansion with respect to slow time and APS theory, the influences of the slowly varying and randomly fluctuating parts of the atmosphere are analyzed, respectively. Currently, there are two main types of atmospheric compensation algorithms: autofocus-based and subaperture-division-based algorithms. The clutter effect caused by the internal movement of the target is still a research focus in NZI GEO SAR studies. The GEO InSAR/D-InSAR theory framework under complex SAR geometries has also been established. European and Chinese scholars have employed GB SAR and Beidou IGSO satellites to carry out equivalent experiments, and a series of results have been obtained. Beside the above research for solving key issues, some novel GEO SAR configurations, mainly the multi-platform GEO SAR represented by GEO SA-BSAR, have entered a stage of rapid theoretical demonstration.

In the near future, GEO SAR's advantages, including a short revisit time and wide coverage, will serve to maintain its prominence as a research focus in both academic and industrial circles. Represented by the Hydroterra concept, GEO SAR will become an important sensor for many scientific applications, such as hydrosphere and geosphere observations. After the launch of China's inclined GEO SAR, based on measured data, the application of short temporal baseline data will quickly become a popular research interest for scholars. Finally, GEO SA-BSAR and FF-GEO SAR are still systems worth exploring due to their irreplicable performances.

Declaration of Competing Interest

The authors declare that they have no conflicts of interest.

Acknowledgments

This work was funded in part by the National Natural Science Foundation of China under Grant Nos. 61960206009, 61971039, and 61971037, the Distinguished Young Scholars of Chongqing (Grant No. cstc2020jcyj-jqX0008), the National Ten Thousand Talents Program 'Young Top Talent' (Grant No. W03070007), the Special Fund for Research on National Major Research Instruments (NSFC Grant Nos. 61827901, 31727901), and the Young Elite Scientists Sponsorship Program by CAST (2017QNRC001).The authors would like to thank Chang Cui, Jiaqi Hu, Yi Sui, Tianyi Zhang, Xinyan Chen and Yuhui Xie for providing the supporting materials related to the sections on bistatic SAR, main disturbance factors, echo focusing and some graphs.

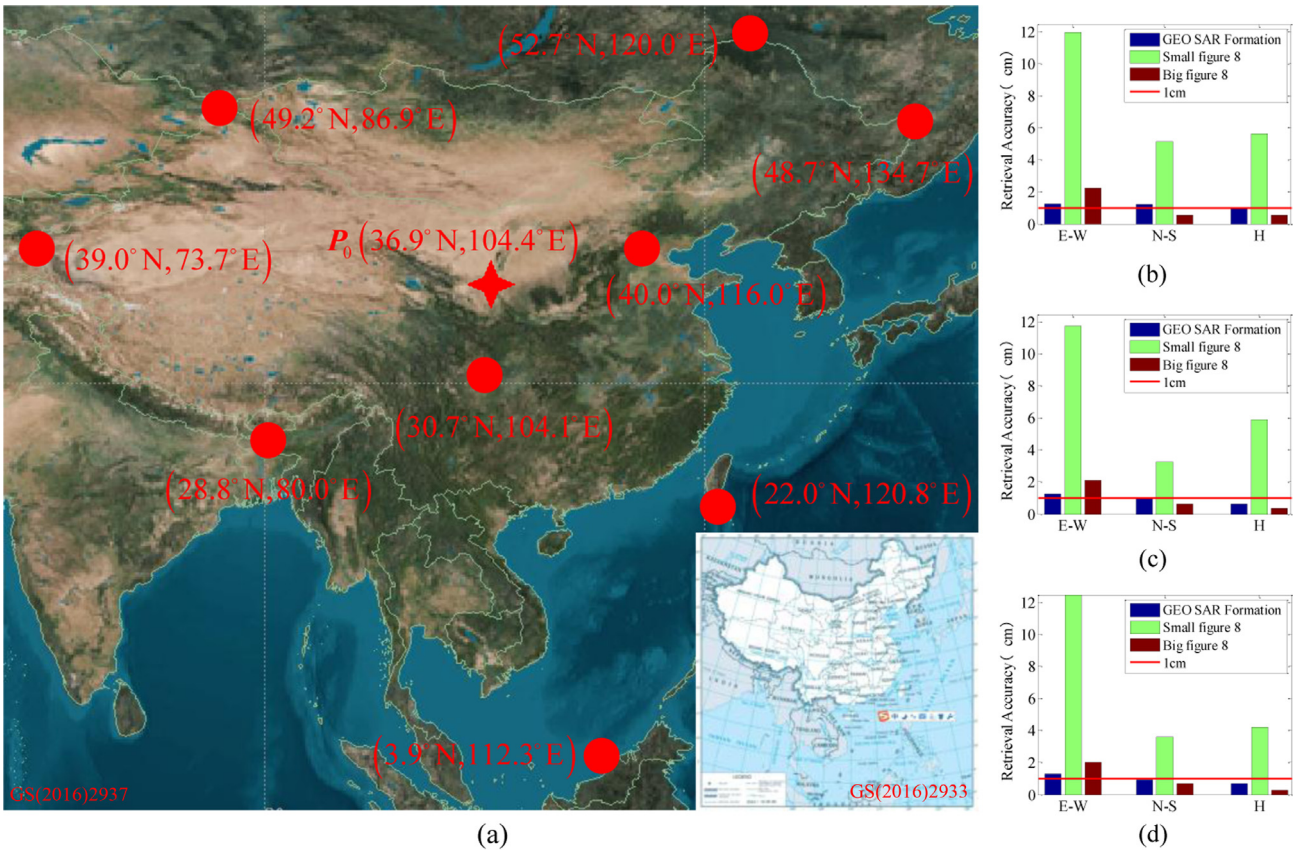

Fig. 13. Formation design and initial performance analysis of the 3D deformation retrieval mission. (a) Points selected for designing the LAN of GEO3. The star P_0 indicates the point for PDOP evaluation and all the dots indicate the points used for incidence angle calculation. (b)-(d): Deformation retrieval accuracy assessments for Beijing, Guangzhou and Xi'an, respectively.

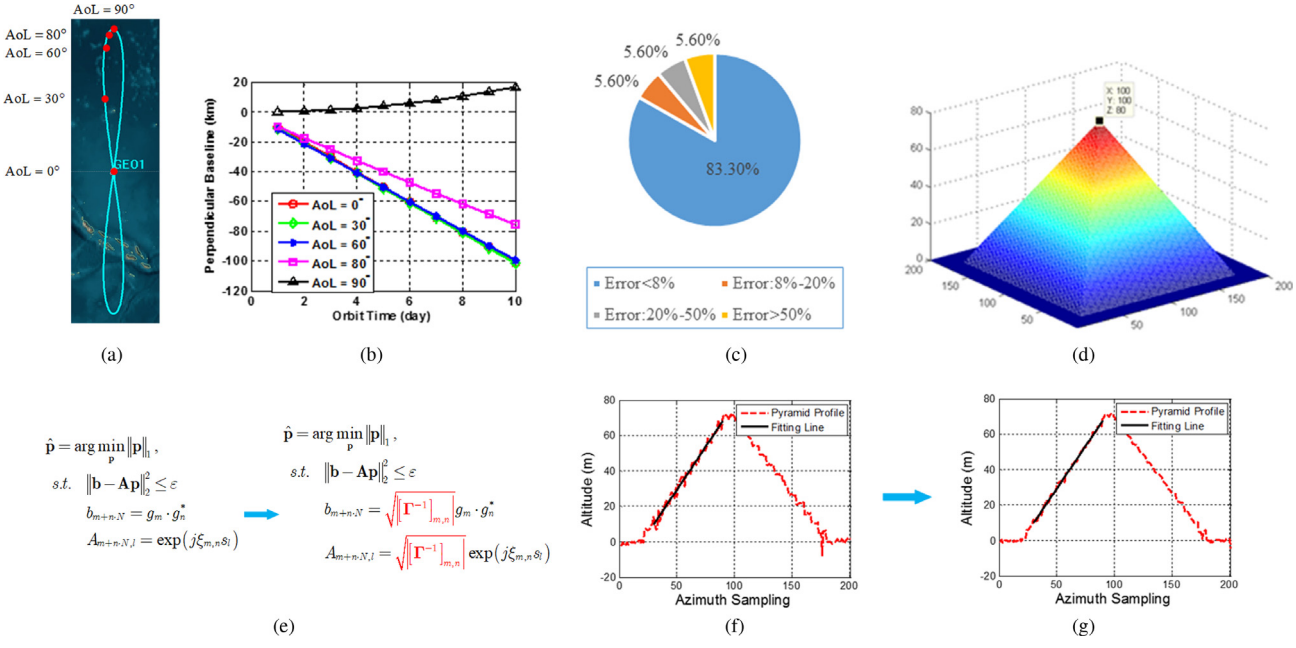

Fig. 14. Research on FF-GEO coherence-based TomoSAR. (a) Orbit positions of several AoLs. (b) Perpendicular baseline for the designed formation. (c) Error distribution of the designed perpendicular baseline. (d) The scene used for simulating the tomography processing methods. (e) (left) Traditional CS method for coherence-based TomoSAR, where $\mathbf{p}$ is the reflectivity, ε is a threshold determined by noise level, $\xi_{m,n} = 4\pi/\lambda \cdot b_{m,n}$ is the wavenumber defined by the perpendicular baseline $b_{m,n}$ of m-th and n-th observation. The whole elevation interval is divided into grids and s_l is the lth one. (right) The improved CS method. (f) Azimuthal slice of the traditional CS method. (g) Azimuthal slice of the improved CS method.

References

[1] A. Moreira, P. Prats-Iraola, M. Younis, et al., A tutorial on synthetic aperture radar, IEEE Geosci. Remote Sens. Mag. 1 (1) (2013) 6–43.
[2] C.H. Gierull, D. Cerutti-Maori, J. Ender, Ground moving target indication with tandem satellite constellations, IEEE Geosci. Remote Sens. Lett. 5 (4) (2008) 710–714.
[3] G. Krieger, et al., TanDEM-X: a satellite formation for high-resolution SAR interferometry, IEEE Trans. Geosci. Remote Sens. 45 (11) (2007) 3317–3341.
[4] R. Hanssen, Radar Interferometry Data Interpretation Error Anal. (2001).
[5] K. Tomiyasu, Tutorial review of synthetic-aperture radar (SAR) with applications to imaging of the ocean surface, Proc. IEEE 66 (5) (1978) 563–583.
[6] P. Snoeij, et al., Sentinel-1, the GMES radar mission, in: 2008 IEEE Radar Conference, 2008, pp. 1–5.
[7] A. Moreira, et al., Tandem-L: a highly innovative bistatic SAR mission for global observation of dynamic processes on the earth\"s surface, Geosci. Remote Sens. Mag. IEEE 3 (2) (2015) 8–23.
[8] T. Long, C. Hu, Z. Ding, et al., Geosynchronous SAR: System and Signal Processing, Springer, 2018.
[9] S. Hobbs, C. Mitchell, B. Forte, et al., System design for geosynchronous synthetic aperture radar missions, IEEE Trans. Geosci. Remote Sens. 52 (12) (2014) 7750–7763.
[10] K. Tomiyasu, Synthetic aperture radar in geosynchronous orbit, 1978 Antennas and Propagation Soc. Int. Symp. 16 (1978) 42–45.
[11] C. Prati, F. Rocca, D. Giancola, et al., Passive geosynchronous SAR system reusing backscattered digital audio broadcasting signals, IEEE Trans. Geosci. Remote Sens. 36 (6) (1998) 1973–1976.
[12] S. Hobbs, GeoSAR: Summary of the Group Design Project MSc in Astronautics and Space Engineering 2005/06, Cranfield University, 2006.
[13] R.M. Fuster, M.F. Usón, A.B. Ibars, Interferometric orbit determination for geostationary satellites, Sci. China Inf. Sci. 60 (6) (2017) 060302.
[14] A.M. Guarnieri, F. Rocca, Options for continuous radar Earth observations, Sci. China Inf. Sci. 60 (6) (2017) 060301.
[15] S. Hobbs, J.P. Sanchez, Laplace plane and low inclination geosynchronous radar mission design, Sci. China Inf. Sci. 60 (6) (2017) 060305.
[16] J.R. Rodon, A. Broquetas, A.M. Guarnieri, et al., Geosynchronous SAR focusing with atmospheric phase screen retrieval and compensation, IEEE Trans. Geosci. Remote Sens. 51 (8) (2013) 4397–4404.
[17] A.V. MONTI-GUARNIERI, et al., Geosynchronous SAR for Terrain & atmosphere with short revisit (GeoSTARe), in: Living Planet Symposium 2016, European Space Agency, 2016, pp. 1–7.
[18] S.E. Hobbs, A. Monti-Guarnieri, Geosynchronous continental land-atmosphere sensing system (G-Class): persistent radar imaging for earth science, in: IGARSS 2018 - 2018 IEEE International Geoscience and Remote Sensing Symposium, 2018, pp. 8621–8624.
[19] R. Haagmans, et al., Earth explorer 10 candidate mission hydroterra, ESA Report Assessment (2020).
[20] M. Lagasio, A.N. Meroni, G. Boni, et al., Meteorological osses for new zenith total delay observations: Impact assessment for the hydroterra geosynchronous satellite on the october 2019 genoa event, Remote Sensing 12 (22) (2020) 3787.
[21] K. Tomiyasu, J.L. Pacelli, Synthetic aperture radar imaging from an inclined geosynchronous orbit, IEEE Trans. Geosci. Remote Sens. GE-21 (3) (1983) 324–329.
[22] S.N. Madsen, W. Edelstein, L.D. DiDomenico, et al., A geosynchronous synthetic aperture radar; for tectonic mapping, disaster management and measurements of vegetation and soil moisture, in: IGARSS 2001. Scanning the Present and Resolving the Future. Proceedings. IEEE 2001 International Geoscience and Remote Sensing Symposium (Cat. No.01CH37217), 1, 2001, pp. 447–449. vol.1.
[23] J. NAsA, Global earthquake satellite system: a 20-year plan to enable earthquake prediction, Technol. Report JPL (2003) 400–1069.
[24] C. Hu, Y. Li, X. Dong, et al., Optimal 3D deformation measuring in inclined geosynchronous orbit SAR differential interferometry, Sci. China Inf. Sci. 60 (6) (2017) 060303.
[25] Z. Chen, X. Dong, Y. Li, et al., Formation design for single-pass GEO InSAR considering earth rotation based on coordinate rotational transformation, Remote Sens. 12 (3) (2020) 573.
[26] Q. Liu, W. Hong, W. Tan, et al., An improved polar format algorithm with performance analysis for geosynchronous circular SAR 2D imaging, Prog. Electromag. Res. 119 (2011) 155–170.
[27] Z. Ding, W. Yin, T. Zeng, et al., Radar parameter design for geosynchronous SAR in squint mode and elliptical orbit, IEEE J.. Sel. Topics Appl. Earth Observ. Remote Sens. 9 (6) (2016) 2720–2732.
[28] H. Cheng, L. Xiaorui, L. Teng, et al., GEO SAR interferometry: theory and feasibility study, in: IET International Radar Conference 2013, 2013, pp. 1–5.
[29] C. Hu, T. Long, T. Zeng, et al., The accurate focusing and resolution analysis method in geosynchronous SAR, IEEE Trans. Geosci. Remote Sens. 49 (10) (2011) 3548–3563.
[30] C. Hu, T. Long, Z. Liu, et al., An improved frequency domain focusing method in geosynchronous SAR, IEEE Trans. Geosci. Remote Sens. 52 (9) (2014) 5514–5528.
[31] J. Ruiz-Rodon, A. Broquetas, E. Makhoul, et al., Nearly zero inclination geosynchronous SAR mission analysis with long integration time for earth observation, IEEE Trans. Geosci. Remote Sens. 52 (10) (2014) 6379–6391.
[32] T. Long, X. Dong, C. Hu, et al., A new method of zero-doppler centroid control in GEO SAR, IEEE Geosci. Remote Sens. Lett. 8 (3) (2011) 512–516.
[33] Q. Zhang, W. Yin, Z. Ding, et al., An optimal resolution steering method for geosynchronous orbit SAR, IEEE Geosci. Remote Sens. Lett. 11 (10) (2014) 1732–1736.
[34] J. Zhang, Z. Yu, P. Xiao, A novel antenna beam steering strategy for GEO SAR staring observation, Geoscience & Remote Sensing Symposium, 2016.
[35] Y. Liu, et al., Echo model analyses and imaging algorithm for high-resolution SAR on high-speed platform, IEEE Trans. Geosci. Remote Sens. 50 (3) (2012) 933–950.
[36] C.P. Li, H.T. Zhang, X.M. Tan, An improved CS algorithm for geosynchronous SAR, J. Astronau. 32 (1) (2011) 179–186.
[37] D. Li, M. Wu, Z. Sun, et al., Modeling and processing of two-dimensional spatial–variant geosynchronous SAR data, IEEE Journal of Selected Topics in Applied Earth Observations and Remote Sensing 8 (8) (2015) 3999–4009.
[38] Y.L. Neo, F. Wong, I.G. Cumming, A two-dimensional spectrum for bistatic SAR processing using series reversion, IEEE Geosci. Remote Sens. Lett. 4 (1) (2007) 93–96.
[39] C. Hu, T. Long, Y. Tian, An improved nonlinear chirp scaling algorithm based on curved trajectory in geosynchronous SAR, Prog. Electromag. Res. 135 (2013) 481–513.
[40] C. Hu, Z. Liu, T. Long, An improved CS algorithm based on the curved trajectory in geosynchronous SAR, IEEE J. Sel. Topics Appl. Earth Observ. Remote Sens. 5 (3) (2012) 795–808.
[41] M. Bao, M.D. Xing, Y.C. Li, Chirp scaling algorithm for GEO SAR based on fourth-order range equation, Electron. Lett. 48 (1) (2012) 41–42.
[42] T. Zeng, W. Yang, Z. Ding, et al., A refined two-dimensional nonlinear chirp scaling algorithm for geosynchronous earth orbit SAR, Prog. Electromag. Research 143 (2013) 19–46.
[43] Z. Ding, B. Shu, W. Yin, et al., A modified frequency domain algorithm based on optimal azimuth quadratic factor compensation for geosynchronous SAR imaging, IEEE J. Sel. Topics Appl. Earth Observ. Remote Sens. 9 (3) (2016) 1119–1131.
[44] B. Hu, Y. Jiang, S. Zhang, et al., Generalized omega-K algorithm for geosynchronous SAR image formation, IEEE Geosci. Remote Sens. Lett. 12 (11) (2015) 2286–2290.
[45] S. Guang-Cai, X. Mengdao, W. Yong, et al., A 2-D space-variant chirp scaling algorithm based on the RCM equalization and subband synthesis to process geosynchronous SAR Data, IEEE Trans. Geosci. Remote Sens. 52 (8) (2014) 4868–4880 08/.
[46] J. Chen, et al., A TSVD-NCS algorithm in range-doppler domain for geosynchronous synthetic aperture radar, IEEE Geosci. Remote Sens. Lett. 13 (11) (2016) 1631–1635.
[47] T. Zhang, Z. Ding, W. Tian, et al., A 2-D nonlinear chirp scaling algorithm for high squint GEO SAR imaging based on optimal azimuth polynomial compensation, IEEE J. Sel. Topics Appl. Earth Observ. Remote Sens. 10 (12) (2017) 5724–5735.
[48] D. Bruno, S.E. Hobbs, Radar imaging from geosynchronous orbit: temporal decorrelation aspects, IEEE Trans. Geosci. Remote Sens. 48 (7) (2010) 2924–2929.
[49] L. Liang, H. Jun, M. Feng, et al., Study on ionospheric effects induced by spatio-temporal variability on medium-earth-orbit SAR imaging quality, J. Electron. Inf. Technol. 36 (4) (2014) 915–922.
[50] C. Hu, Y. Tian, X. Yang, et al., Background ionosphere effects on geosynchronous SAR focusing: theoretical analysis and verification based on the BeiDou navigation satellite system (BDS), IEEE J. Sel. Topics Appl. Earth Observ. Remote Sens. 9 (3) (2015) 1143–1162.
[51] Y. Tian, et al., Theoretical analysis and verification of time variation of background ionosphere on geosynchronous SAR imaging, IEEE Geosci. Remote Sens. Lett. 12 (4) (2014) 721–725.
[52] X. Dong, C. Hu, W. Tian, et al., Design of validation experiment for analysing impacts of background ionosphere on geosynchronous SAR using GPS signals, Electron. Lett. 51 (20) (2015) 1604–1606.
[53] C. Hu, Y. Li, X. Dong, et al., Impacts of temporal-spatial variant background ionosphere on repeat-track GEO D-InSAR system, Remote Sens. 8 (11) (2016) 916.
[54] C. Hu, Y. Li, X. Dong, et al., Performance analysis of L-band geosynchronous SAR imaging in the presence of ionospheric scintillation, IEEE Trans. Geosci. Remote Sens. 55 (1) (2016) 159–172.
[55] X. Dong, Y. Li, T. Ye, Analysis of ionospheric scintillation impacts on GEO SAR focusing, J. Signal Process. 31 (2) (2015) 226–232.
[56] Y. Li, C. Hu, X. Dong, et al., Impacts of ionospheric scintillation on geosynchronous SAR focusing: preliminary experiments and analysis, Sci. China Inf. Sci. 58 (10) (2015) 1–3.
[57] Y. Ji, Q. Zhang, Y. Zhang, et al., L-band geosynchronous SAR imaging degradations imposed by ionospheric irregularities, Sci. China Inf. Sci. 60 (6) (2017) 060308.
[58] J. Hu, C. Hu, D. Zhang, et al., Impacts of drifting ionospheric irregularities on inclined geosynchronous SAR, in: 2019 6th Asia-Pacific Conference on Synthetic Aperture Radar (APSAR), IEEE, 2019, pp. 1–4.
[59] Y. Ji, Y. Zhang, Z. Dong, et al., Impacts of ionospheric irregularities on L-band geosynchronous synthetic aperture radar, IEEE Trans. Geosci. Remote Sens. (2020).
[60] Y. Li, et al., Ionospheric scintillation impacts on L-band geosynchronous D-InSAR system: models and analysis, IEEE J. Sel. Topics Appl. Earth Observ Remote Sens. 11 (12) (2018) 4862–4873.
[61] C. Hu, Y. Li, X. Dong, et al., Avoiding the ionospheric scintillation interference on geosynchronous SAR by orbit optimization, IEEE Geosci. Remote Sens. Lett. 13 (11) (2016) 1676–1680.
[62] R. Wang, H. Cheng, Y. Li, et al., Joint amplitude-phase compensation for ionospheric scintillation in GEO SAR imaging, IEEE Trans. Geosci. Remote Sens. 55 (6) (2017) 3454–3465.
[63] L. Kou, M. Xiang, X. Wang, et al., Tropospheric effects on L-band geosynchronous circular SAR imaging, IET Radar, Sonar & Navigation 7 (6) (2013) 693–701.
[64] A.M. Guarnieri, F. Rocca, A.B. Ibars, Impact of atmospheric water vapor on the design of a Ku band geosynchronous SAR system, 2009 IEEE international geoscience and remote sensing symposium, 2, 2009 II-945-II-948.
[65] T. Ye, X.C. Dong, H.U. Cheng, et al., Analysis of troposphere impacts on geosynchronous SAR imaging, J. Signal Process. (2015).

[66] A.M. Guarnieri, A. Leanza, A. Recchia, et al., Atmospheric phase screen in GEO-SAR: estimation and compensation, IEEE Trans. Geosci. Remote Sens. 56 (3) (2018) 1668–1679.
[67] X. Dong, J. Hu, C. Hu, et al., Modeling and quantitative analysis of tropospheric impact on inclined Geosynchronous SAR imaging, Remote Sens. 11 (7) (2019) 803.
[68] W. Sheng, S.E. Hobbs, Research on compensation of motion, Earth curvature and tropospheric delay in GEOSAR, Acta Astronaut. 68 (11) (2011) 2005–2011 2011/06/01/.
[69] D. Bruno, S.E. Hobbs, G. Ottavianelli, Geosynchronous synthetic aperture radar: concept design, properties and possible applications, Acta Astronaut. 59 (1) (2006) 149–156.
[70] J. Ruiz-Rodon, A. Broquetas, E. Makul, A. Monti-Guarnieri, A. Recchia, Internal clutter motion impact on the long integration GEOSAR acquisition, in: 2014 IEEE Geoscience and Remote Sensing Symposium, 2014, pp. 2343–2346.
[71] A. Monti-Guarnieri, M. Manzoni, D. Giudici, et al., Vegetated target decorrelation in SAR and interferometry: models, simulation, and performance evaluation, Remote Sens. 12 (16) (2020) 2545.
[72] A. Recchia, A.M. Guarnieri, A. Broquetas, et al., Impact of scene decorrelation on geosynchronous SAR data focusing, IEEE Trans. Geosci. Remote Sens. 54 (3) (2015) 1635–1646.
[73] C. Convenevole, S. Hobbs, Method for estimating clutter limited geosynchronous synthetic aperture radar performance, in: 2019 International Radar Conference (RADAR), IEEE, 2019, pp. 1–6.
[74] Y. Li, A.M. Guarnieri, C. Hu, et al., Performance and requirements of GEO SAR systems in the presence of radio frequency interferences, Remote Sens. 10 (1) (2018).
[75] A. Leanza, M. Manzoni, A. Monti-Guarnieri, et al., LEO to GEO-SAR interferences: modelling and performance evaluation, Remote Sens. 11 (14) (2019) 1720.
[76] L. Teng, Z. Tianyi, D. Zegang, et al., Effect analysis of antenna vibration on GEO SAR image, IEEE Trans. Aerosp. Electron. Syst. 56 (3) (2020) 1708–1721 06/.
[77] C. Hu, Y. Li, X. Dong, et al., Optimal data acquisition and height retrieval in repeat-track geosynchronous SAR interferometry, Remote Sensing 7 (10) (2015) 13367–13389.
[78] C. Hu, Y. Li, X. Dong, et al., Three-dimensional deformation retrieval in geosynchronous SAR by multiple-aperture interferometry processing: theory and performance analysis, IEEE Trans. Geosci. Remote Sens. 55 (11) (2017) 6150–6169.
[79] X. Dong, C. Hu, W. Tian, et al., Feasibility study of inclined geosynchronous SAR focusing using Beidou IGSO signals, Sci. China Inf. Sci. 59 (12) (2016) 129302.
[80] F. Liu, X. Fan, T. Zhang, et al., GNSS-based SAR interferometry for 3-D deformation retrieval: algorithms and feasibility study, IEEE Trans. Geoence. Remote Sens. 56 (99) (2018) 5736–5748.
[81] C. Hu, B. Zhang, X. Dong, et al., Geosynchronous SAR tomography: theory and first experimental verification using beidou IGSO satellite, IEEE Trans. Geosci. Remote Sens. 57 (9) (2019) 6591–6607.
[82] H. Xu, L. Huang, X. Qiu, et al., A new geosynchronous SAR constellation and its signal characteristics, IEEE Access 7 (2019) 101539–101551.
[83] G.L. Guttrich, W.E. Sievers, N.M. Tomljanovich, Wide area surveillance concepts based on geosynchronous illumination and bistatic unmanned airborne vehicles or satellite reception, in: Proceedings of the 1997 IEEE National Radar Conference, 1997, pp. 126–131.
[84] S. Ghaleb, F.A. Kinder, (2010). U.S. Patent No. 7,710,313. Washington, DC: U.S. Patent and Trademark Office.
[85] J.B. Zheng, H.J. Song, X.Q. Shong, et al., An algorithm based on spectrum shift for improving range resolution using GEO spaceborne\/airborne multistatic SAR, J. Electron. Inf. Technol. (2010).
[86] Z. Sun, J. Wu, J. Pei, et al., Inclined geosynchronous spaceborne–airborne bistatic SAR: performance analysis and mission design, IEEE Trans. Geosci. Remote Sens. 54 (1) (2016) 343–357.
[87] Z. Sun, J. Wu, J. Yang, et al., Path planning for GEO-UAV bistatic SAR using constrained adaptive multiobjective differential evolution, IEEE Trans. Geosci. Remote Sens. 54 (11) (2016) 6444–6457.
[88] Y. Yuan, Y. Hao, L. Ling, et al., An imaging method of GEO spaceborne-airborne bistatic SAR, Radar Ence Technol. (2007).
[89] L. Ling, Y.Q. Zhou, J. Li, et al., Synchronization of Geo Spaceborne-Airborne Bistatic SAR, IGARSS 2008 - 2008 IEEE International Geoscience and Remote Sensing Symposium, 2008 vol. 3, pp. III - 1209-III - 1211.
[90] J. Wu, Z. Sun, H. An, et al., Azimuth signal multichannel reconstruction and channel configuration design for geosynchronous spaceborne-airborne bistatic SAR, IEEE Trans. Geosci. Remote Sens. (2018) 1–12.
[91] H. An, J. Wu, Z. He, et al., Geosynchronous spaceborne–airborne multichannel bistatic SAR imaging using weighted fast factorized backprojection method, IEEE Geosci. Remote Sens. Lett. 16 (10) (2019) 1590–1594.
[92] H. An, J. Wu, Z. Sun, et al., A two-step nonlinear chirp scaling method for multichannel GEO spaceborne–airborne bistatic SAR spectrum reconstructing and focusing, IEEE Trans. Geosci. Remote Sens. 57 (6) (2019) 3713–3728.
[93] Z. Sun, J. Wu, Z. Li, et al., Geosynchronous spaceborne-airborne bistatic SAR data focusing using a novel range model based on one-stationary equivalence, IEEE Trans. Geosci. Remote Sens. (2020) 1–17.
[94] H.Y. Shi, Y.Q. Zhou, J. Chen, An algorithm of GEO spaceborne-airborne bistatic three-channel SAR ground moving target indication, J. Electron. Inf. Technol. (2009).
[95] X. Dong, C. Cui, Y. Li, et al., Geosynchronous spaceborne-airborne bistatic moving target indication system: performance analysis and configuration design, Remote Sensing 12 (11) (2020).
[96] Y. Zhang, W. Xiong, X. Dong, et al., A novel azimuth spectrum reconstruction and imaging method for moving targets in geosynchronous spaceborne–airborne bistatic multichannel SAR, IEEE Trans. Geosci. Remote Sens. 58 (8) (2020) 5976–5991.
[97] W. Xu, Z.B. Wei, P.P. Huang, et al., Azimuth multichannel reconstruction for moving targets in geosynchronous spaceborne-airborne bistatic SAR, Remote Sensing 12 (11) (2020).
[98] H. An, J. Wu, K.C. Teh, et al., Simultaneous moving and stationary target imaging for geosynchronous spaceborne-airborne bistatic SAR based on sparse separation, IEEE Trans. Geosci. Remote Sens. (2020) 1–14.
[99] A.M. Guarnieri, S. Tebaldini, F. Rocca, A. Broquetas, GEMINI: geosynchronous SAR for earth monitoring by interferometry and imaging, in: 2012 IEEE International Geoscience and Remote Sensing Symposium, 2012, pp. 210–213.
[100] A.M. Guarnieri, et al., ARGOS: a fractioned geosynchronous SAR, Acta Astronaut. (2015).
[101] A.M. Guarnieri, A. Broquetas, A. Recchia, et al., Advanced radar geosynchronous observation system: ARGOS, IEEE Geosci. Remote Sens. Lett. 12 (7) (2015) 1406–1410.
[102] B.J. Zhoo, Q.G. Zhong, C. Dai, et al., Baseline designing and implementation approach for a Geo-SAR tomography system, J. Eng. (2019).
[103] M. Nannini, M. Martone, P. Rizzoli, et al., Coherence-based SAR tomography for spaceborne applications, Remote Sens. Environ. 225 (2019) 107–114.

Cheng Hu received the B.S. degree in electronic engineering from the National University of Defense Technology, Changsha, China, in 2003, and the Ph.D. degree in target detection and recognition from the Beijing Institute of Technology (BIT), Beijing, China, in 2009. He was a Visiting Research Associate with the University of Birmingham, Birmingham, U.K., for 15 months from 2006 to 2007. Since September 2009, he has been with the School of Information and Electronics, BIT, and promoted to be a Full Professor in 2014, a Doctoral Supervisor, and the Vice-Director of the Radar Research Lab. He has authored a monograph on the topic of Geosynchronous Synthetic Aperture Radar (published by Springer), over 100 SCI-indexed journal articles and over 100 conference articles. His main research interests include new concept synthetic aperture radar imaging and the biological detection radar system and signal processing.

Zhiyang Chen was born in Fujian, China, in 1993. He received the B.S. degree in the Department of Electronic Engineering from Tsinghua University, Beijing, China, in 2016. He is currently pursuing the Ph.D. degree in the School of Information and Electronics from Beijing Institute of Technology, Beijing, China. His research interests include geosynchronous synthetic aperture radar (GEO SAR) satellites formation design, SAR interferometry and SAR tomography.